NASA TECHNICAL NOTE

NASA TN D-2399

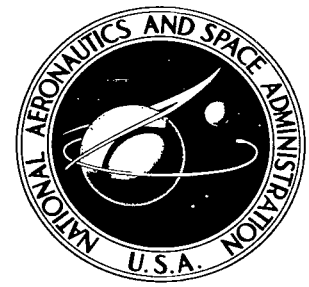

NASA TN D-2399

EXPERIMENTAL AND ANALYTICAL INVESTIGATION OF PROPELLER WHIRL FLUTTER OF A POWER PLANT ON A FLEXIBLE WING

by Robert M. Bennett and Samuel R. Bland

Langley Research Center
Langley Station, Hampton, Va.

NATIONAL AERONAUTICS AND SPACE ADMINISTRATION • WASHINGTON, D. C. • AUGUST 1964

EXPERIMENTAL AND ANALYTICAL INVESTIGATION OF PROPELLER WHIRL FLUTTER OF A POWER PLANT ON A FLEXIBLE WING

By Robert M. Bennett and Samuel R. Bland

Langley Research Center
Langley Station, Hampton, Va.

NATIONAL AERONAUTICS AND SPACE ADMINISTRATION

For sale by the Office of Technical Services, Department of Commerce,
Washington, D.C. 20230 -- Price $1.75

EXPERIMENTAL AND ANALYTICAL INVESTIGATION OF PROPELLER WHIRL FLUTTER OF A POWER PLANT ON A FLEXIBLE WING

By Robert M. Bennett and Samuel R. Bland
Langley Research Center

SUMMARY

Results of an investigation of propeller whirl flutter are presented for a model consisting of a single propeller and simulated power plant mounted with flexibility in pitch and yaw to a cantilevered, semispan wing. Several configurations differing in the power-plant parameters were investigated analytically and experimentally. An analysis is presented employing four uncoupled modes: wing bending, wing torsion, power-plant pitch, and power-plant yaw. Experimental results are compared with this four-mode analysis and with an analysis including only power-plant freedoms.

The experimental and analytical results indicate that the effects of the wing on the whirl flutter boundary were large for some cases, depending on the system parameters, and were generally stabilizing for the configurations considered. The four-mode analysis generally gave better results than the two-mode analysis, but only gave fair agreement in some instances. The analyses indicated that in cases of large-amplitude wing motion, wing aerodynamics can have significant stabilizing effects.

INTRODUCTION

A design consideration for propeller-driven aircraft is the prevention of a dynamic instability, generally termed propeller whirl flutter or autoprecession, in which the propeller hub wobbles or executes a whirling motion. The flutter for an isolated power plant has been treated analytically in references 1 to 7. Comparisons of measured and calculated flutter boundaries for a windmilling propeller (ref. 8) indicated that the whirl-flutter boundary could be satisfactorily predicted if accurate aerodynamic parameters were used. Calculations for thrusting propellers in the cruise condition (refs. 1 to 4) have indicated little effect of thrust on whirl flutter. However, the question of the effects of the wing has been considered only briefly in these investigations. Furthermore, comparison of the theoretical results of reference 1 for an isolated power plant with the data of reference 9 for a four-engine model indicated large differences that might be attributed to the wing and complete

model. Since further investigation of the effects of the wing was desirable, the present investigation was undertaken with the following objectives:

(1) To determine the whirl-flutter boundaries of a power plant (with windmilling propeller) on a cantilever, semispan wing, which not only has realistic parameters but is also more readily amenable to analysis and physical interpretation than a complicated four-engine model.

(2) To investigate the system of reference 8 on the semispan wing and evaluate the range of applicability of the theory for an isolated power plant in a limited manner.

(3) To analyze combined wing and power-plant flutter, evaluate the analysis, and explore the dynamics of wing—power-plant coupling.

For this investigation the model of reference 8 was mounted on a cantilevered semispan wing having an aspect ratio of 6.97 (based on area of exposed wing panel) and a taper ratio of 0.430. Flutter boundaries were measured over a range of power-plant stiffnesses and damping levels and propeller blade angles. In addition, three other configurations differing in power-plant parameters were investigated over a range of blade angles for a single value of stiffness and of damping. Following the list of symbols in appendix A, the equations of motion are developed in appendix B for coupled wing—power-plant flutter by using an uncoupled-mode analysis and by omitting aerodynamic coupling between the wing and propeller. The results of this analysis are compared with the results of the experiment and with the theory for an isolated power plant. The effects of gyroscopic coupling on the natural vibration modes are briefly considered in appendix C.

APPARATUS AND TESTS

Tunnel

The investigation was made in the Langley transonic dynamics tunnel which is a slotted-throat, variable-pressure, single-return wind tunnel having a test section 16 feet square (with cropped corners). It is capable of operation at Mach numbers up to 1.2 and at stagnation pressures from near vacuum to slightly above atmospheric. Either air or freon can be used as a test medium. Large windows are provided for close, unobstructed viewing of the model. The dynamic pressure in the test section can be rapidly reduced when flutter occurs by the operation of a bypass valve in a channel which connects the plenum chamber surrounding the test section to the return passage of the tunnel.

The present investigation was conducted in air at near atmospheric conditions and at Mach numbers less than 0.3.

Model

General arrangement and mounting.- The model consisted of a semispan wing with a single nacelle—power-plant combination with windmilling propeller. Although no attempt was made to scale the model from a specific airplane, the model parameters are believed to be realistic since the model was adapted from the four-engine model of reference 9. The model was cantilevered from the tunnel wall as shown in an overall view in figure 1. This was accomplished by sandwiching the root portion of the wing spar with heavy plates (see fig. 2), bolting them together, and clamping the assembly in a remotely operable turntable, which was used to adjust the angle of attack of the model (see section entitled "Tests"). In order to minimize effects of the wall boundary layer and to fair around the rigid inboard portion of the wing, a simulated fuselage was bolted to the tunnel wall. Sealing around the wing-fuselage juncture was accomplished by means of a flexible foam material.

Simulated power plant.- Four configurations, differing in the parameters of the simulated power plant, were tested and are denoted herein as configurations A, B, C, and D. The system consisted of a simulated engine and a propeller attached to an aluminum mounting beam through a gimbal with spring-restrained pitch and yaw freedoms. A variable-speed motor with an eccentrically mounted weight on its shaft formed part of the engine mass and served as a shaker device for configurations A and B. The schematic for each configuration is given in figure 3. Configuration A was the symmetrical model of reference 8. Configuration B differed from configuration A only in the location of the lead weights, which were moved from the rear of the engine to the mounting beam at the same distance from the elastic axis (fig. 3(a)). For configuration C, the simulated engine mass was also removed from the gimbal structure and mounted on the mounting beam at the same distance from the elastic axis (fig. 3(b)). Configuration D differed from configuration C in the spring and clip arrangements which permitted unequal pitch and yaw stiffnesses. The mass parameters for each configuration are given in table I.

The aluminum beam of this model on which the gimbal was mounted was similar to that of reference 9, but was stiffened to raise its frequencies considerably above the whirl-flutter frequencies by the addition of L-section doublers (fig. 3). For example, cantilever frequencies of the mounting beam with engine-propeller configuration A were 29 cps in pitch and 24 cps in yaw.

The nacelle was made of balsa construction and was fixed to the wing beam with a stiff mounting bracket. Clearance for whirling motions was left between the nacelle and spinner.

The four-blade aluminum propeller was that used for the investigation of references 8 and 9. The variation of windmilling advance ratio V/nD with reference blade angle is given in figure 4 (from ref. 8).

Wing.- The wing, shown in figure 2, consisted of a built-up aluminum spar for stiffness and balsa pods for airfoil contour. The gaps between the pods were sealed with flexible, foam plastic strips. For analysis purposes, the root was considered to be fixed at the bolts through the outboard edge of the sandwiching plates, 1.7 inches inboard of the edge of the first pod. The rounded

tip was treated as a streamwise tip ending at the tip of the wing spar (fig. 2). The aspect ratio was 6.97 (based on area of the exposed wing panel) and the taper ratio was 0.430. The center line of the wing spar, which was the elastic axis, was swept forward 4.9°. The nondimensional distance from the midchord to the elastic axis is shown in figure 5.

Although the elastic axis was swept forward, the pods were formed as streamwise strips (fig. 2). The mass, static unbalance, and inertia about the elastic axis of each strip were measured in the streamwise direction at the spanwise position of the center of gravity of the strip, and were considered to be the average values over the width of the strip. (The measurements for the spar were made on a similar wing spar cut into strips.) The spanwise distributions of these parameters are presented in figure 6 in which the nondimensional parameters are based on the streamwise semichord at the spanwise station of the center of gravity of the strip. The parameters for the propeller, power plant, nacelle, and mounting beam (not included in fig. 6) are presented in table I.

The spanwise distributions of bending and torsional stiffness are presented in figure 7. The stiffness values were obtained by differentiating parabolic approximations of the slope of the static deflection curve for a concentrated load at the tip. The slopes, which were measured with a mirror system and were averaged for several values of loading magnitude, are also presented in figure 7.

Vibration Modes

In order to check the mathematical description of the wing by using the measured physical properties, a series of vibration measurements were made and compared with calculations. For the bare wing spar, which has small static unbalance coupling, measured first and second bending frequencies were 17.6 cps and 59.5 cps, respectively. Corresponding calculated uncoupled frequencies (obtained by the method of ref. 10) were 17.0 cps and 66.4 cps. The calculated first torsional frequency of the bare wing spar was 267 cps; coupled modes were measured at 255 and 270 cps, the latter being more nearly a pure torsion mode.

With the pods added to the wing spar, but the nacelle omitted, the first three measured modes were 10.6 cps (first bending), 39.0 cps (second bending), and 47.0 cps (first torsion). Corresponding calculated frequencies (considering two uncoupled bending modes and one uncoupled torsional mode, all coupled by static unbalance in a Rayleigh-Ritz type analysis) were 11.2 cps, 43.1 cps, and 53.4 cps, respectively. Therefore, the mathematical description of the wing using measured physical properties satisfactorily predicts the measured frequencies of the bare spar or of the wing without the nacelle.

The measured node lines of the first three modes, which involve primarily wing motion, are sketched in figure 8 for the complete model of configuration A with $f_\theta = f_\psi = 9.3$ cps. The calculated uncoupled first bending (10.1 cps) mode shape and first torsional (17.1 cps) mode shape are presented in figure 9. When these two modes are coupled by static unbalance and the engine pitch mode, the calculated coupled frequencies compare with measurements as follows:

Predominant response	Calculated coupled frequency, cps	Measured frequency, cps
Engine pitch, θ	9.2	9.3
Engine yaw, ψ	9.3	9.3
First wing bending, h_1	10.1	10.4
Wing torsion, α	17.4	14.3
Second wing bending, h_2	----	39.1

Good agreement in frequency is obtained for these modes with the exception of the 14.3-cps mode which is primarily wing torsion. The poor agreement for this mode may be a result of considering only two wing modes in the calculations. Although the next coupled mode involving primarily wing motion has a frequency of 39.1 cps, the calculated uncoupled second bending mode frequency is 23.7 cps, and its inclusion could possibly affect the results.

Instrumentation

An automatic digital readout system was used to record the tunnel static and stagnation pressures and stagnation temperature.

The accelerations of the simulated engine mass were determined by linear accelerometers mounted on the nonrotating part of the pivoting mass. The frequency and a qualitative indication of the amplitudes of the wing bending and torsional oscillations were determined by strain gages near the wing root. These data were recorded on a direct writing oscillograph recorder for real-time monitoring of the test. Propeller rotational speed was measured by a magnetic pickup, mounted at the propeller shaft, which drove an electronic counter.

Tests

In the tests of configurations A and B, the tunnel was brought up to a low speed, the model was initially disturbed sinusoidally by the shaker, and the nature of the free vibrations was observed visually and on the oscillograph record. Airstream velocity was then increased by a small increment, and the model again disturbed. This procedure was continued until a sustained, approximately constant amplitude oscillation was produced. The tunnel velocity was then rapidly reduced to prevent model damage. The procedure for configurations C and D was essentially the same; however, since the shaker was ineffective for these configurations random tunnel turbulence served as the flutter excitation. The absence of the shaker did not appear to impair the selection of the flutter condition by the observer. The wing was maintained at nearly zero static tip deflection in bending by varying the angle of attack of the wing with the mounting turntable.

In some cases the stability of the flutter mode was independent of amplitude as indicated by linear theory. However, as in the tests reported in reference 8, cases were encountered in which the amplitude of flutter was limited at a given velocity, and increased with increasing velocity, indicating a nonlinear effect. The wind-off power-plant damping for these cases increased with amplitude. The pertinent damping coefficient was assumed herein, as in reference 8, to be that derived from the records of the decay of free vibration at the amplitude of flutter. Also, there were some instances where unstable oscillations were produced if sufficiently large amplitudes of motion were excited without an increase in velocity. The damping for these cases decreased with increasing amplitude; hence, the appropriate damping coefficient was assumed to be that derived from the decay records at the amplitude where the motion began to be unstable. Damping records were taken before and after each series of runs at a given stiffness or damping level. As the power-plant damping varies somewhat during a series of runs, the accuracy of $2\zeta_i$ is estimated to be about ± 0.005.

Power-plant stiffness and damping levels and propeller blade angle were varied separately for configuration A. (The damping level was adjusted by inserting sponge rubber between the gimbal rings.) Several blade angles, but only one level of stiffness and damping, were investigated for configurations B, C, and D. A summary of test conditions and data is given in table II.

All the flutter tests were made in air at near atmospheric conditions and at Mach numbers less than 0.3.

DESCRIPTION OF ANALYSIS

An analysis of the whirl flutter of a wing—propeller—power-plant combination including wing flexibility is developed in detail in appendix B and is applied herein to the model of this report. The analysis is based on a Lagrangian formulation of the equations of motion employing deflections in four uncoupled vibration modes as generalized coordinates. The system treated analytically is depicted in figure 10. It consists of a single, rigid engine-propeller system mounted with spring-restrained gimbals to a rigid mounting beam which is mounted on the flexible wing. Two vibration modes of the wing, bending and torsion, are considered. These are described as bending and twisting about a straight, unswept elastic axis. Both propeller and wing aerodynamic forces are included; however, aerodynamic interference effects between the wing and propeller, and nacelle aerodynamic forces are neglected. The aerodynamic forces acting on the propeller are expressed in terms of stability derivatives as in references 1, 2, and 8. The modified-strip analysis method of reference 11 is employed to represent the wing aerodynamic forces.

From this analysis the speed for neutral stability (boundary between stable and unstable motion) is determined. This flutter speed, expressed in nondimensional form as $V/R\omega_\theta$, is determined as a function of the damping of the engine pitch mode, $2\zeta_\theta$, by specifying the following damping parameters: g_α, g_h, and $2\zeta_\psi/2\zeta_\theta$. The method of solution and input quantities required are discussed in appendix B. A discussion of the determination of the input quantities for the

model of this report is also given in appendix B. The comparison of the results of the application of this analysis with experiment for the configuration of this report is discussed in the following section.

RESULTS AND DISCUSSION

Remarks on Wing Flutter

A conventional wing flutter analysis as obtained from the flutter determinant (eq. (B43)) by assuming complete rigidity of the power-plant mounting in pitch and yaw and by using the first torsional and bending modes of the wing indicated no flutter solution with or without propeller aerodynamics. It should be pointed out that studies of references 12 and 13 indicate that, in general, more than two uncoupled modes would be required to predict flutter accurately when large concentrated weights are attached to the structure. Furthermore, flexibility in the mounting of a concentrated mass can have an important influence on flutter (ref. 14). However, since the concentrated nacelle mass is located well ahead of the elastic axis - a condition which has been shown to have a strong stabilizing influence on wing flutter (see ref. 15) - it is felt that the present predictions based on a two-mode analysis are at least indicative that classical wing flutter occurs at velocities well above those considered herein. Hence, the primary emphasis in this investigation will be on the effects of the wing on propeller whirl flutter.

Whirl Flutter

The experimental flutter data for configuration A are presented in figure 11 in the form of viscous damping of the power-plant modes required for stability as a function of reduced velocity $V/R\bar{\omega}$ in terms of the average wind-off frequency, $\bar{\omega} = \frac{\omega_\theta + \omega_\psi}{2}$; the stable region is above the boundary. Such a boundary is unique for a given blade angle for flutter of a power plant flexibly mounted on a rigid structure, but becomes a function of the mass, natural frequencies, and damping of the wing for the power plant mounted on a flexible wing. Thus, the power-plant stiffness level is indicated (fig. 11) by the ratio of uncoupled frequencies $\bar{\omega}/\omega_h$. As density varied slightly from one test point to another and the damping in pitch and damping in yaw were not widely different, the damping parameter $2\bar{\zeta} = \frac{2\zeta_\theta + 2\zeta_\psi}{2}\frac{\rho_o}{\rho}$ has been used to adjust the experimental data to a reference density value of 0.0022 slug/cu ft. This relation is an approximate one for the power plant mounted on a rigid structure (ref. 8). The power-plant damping is treated as viscous damping, as better agreement was obtained in reference 8 with viscous damping than with structural damping. However, the damping of the wing modes is considered to be structural damping herein.

The data for configuration A are compared with the theory including only power-plant pitch and yaw freedoms (from ref. 8) and with the theory including four modes: power-plant pitch and yaw, wing bending, and wing torsion for a

power-plant restraint stiffness resulting in a frequency ratio $\bar{\omega}/\omega_h$ of 1.13. A comparison of the data with the theory for two modes shows good agreement for some cases, but only fair for others. It should be noted that the results of reference 8 for an isolated power plant with two degrees of freedom indicated very good agreement between theory and experiment. The theory for four modes (for $\bar{\omega}/\omega_h = 1.13$) shows a stabilizing effect in comparison with the theory for two modes at the lower damping levels and is in very good agreement with the data (for $\bar{\omega}/\omega_h = 1.13$) except at a blade angle of 58°. Appendix C indicates that the regions of large coupling between the whirling modes and the wing modes, as indicated by frequency shifts, are near the coincidences of the frequencies of the whirling modes with those of the coupled modes involving primarily wing motion. The whirl flutter frequencies for configuration A (table II) were lower than those of the first coupled mode; however, for values of $\bar{\omega}$ above the first bending frequency the whirl flutter frequencies were as much as 0.9 of the frequency of the first coupled mode. No consistent effect of the higher whirling frequencies is shown in the data (fig. 11).

The flutter boundaries calculated for configurations B, C, and D including only power-plant pitch and yaw modes are compared with the boundaries calculated including wing bending and torsional modes for three blade angles in figure 12. For configuration D, the presentation is based on $V/R\omega_\theta$ as ω_θ and ω_ψ are widely different (table II). A small stabilizing effect of the wing is predicted for configurations B and D, but a large stabilizing effect is predicted for configuration C at the higher blade angles. Also, for configuration C where the wing is significantly stabilizing, the flutter boundary is less sensitive to damping (fig. 12(b)).

The theoretical flutter speed boundaries employing either two or four modes are compared with experimental data for a single value of power-plant restraint stiffness and damping for each configuration in figure 13. Corresponding values of flutter-frequency ratio are also presented in figure 13. The theoretical values for configuration A, taken from figure 11, show little effect of the wing on the flutter speeds (fig. 13(a)); however, some effect is indicated by the experimental flutter speed at a blade angle of 58°. Calculated flutter frequencies for two- and four-mode analyses differ little and are in good agreement with experiment (fig. 13(a)). For configuration B, the theoretical flutter speed boundary employing four modes is higher than that obtained using two modes, but, as for configuration A, is in good agreement with experiment only at the lower blade angles (fig. 13(b)). Calculated flutter frequencies show little effect of the wing, but are higher than experiment by about 10 to 15 percent (fig. 13(b)). For configuration C, the theoretical flutter boundary employing four modes is considerably higher than that calculated with two modes and is in good agreement with experiment over the range of blade angles investigated experimentally (fig. 13(c)). Flutter frequencies are also in better agreement from the four-mode analysis (fig. 13(c)), but are high by about 10 to 25 percent. Only a small stabilizing effect of the wing is indicated by the four-mode analysis for configuration D (fig. 13(d)). However, both theoretical boundaries are higher than experiment. Calculated flutter frequencies are in good agreement for the two-mode calculations, but are low when four modes are employed (fig. 13(d)).

Thus, for configuration A the wing had a small effect; however, for configurations B and C the wing had a significant stabilizing effect. The addition of the two wing modes to the theory of reference 1 generally improved the agreement of the theory with experiment, particularly for configuration C, but did not fully predict the stabilizing effects or trends. The results of reference 12 showed that the flutter mode shape of a wing with a large concentrated mass could be quite different from the first bending or torsional mode. In particular, the relative amplitude at flutter at the position of the concentrated mass was higher than that for the first bending mode and lower than that for the first torsional mode. Such a result could lead to the observed trends herein, and suggests that inclusion of additional wing modes may be required for better correlation.

In reference 1 a comparison of the theory for the isolated power plant with data of reference 9 indicated the possibility of large stabilizing effects of the wing and complete model. Also, unpublished analytical studies by R. J. Zwaan and H. Bergh of the National Aero-Astronautical Research Institute, N.L.R., Amsterdam, show that generally the wing has a stabilizing effect on whirl flutter, but under certain conditions wing flexibility can give a reduction in the flutter speed.

Although the theory including four modes was generally conservative for configurations A, B, and C, for configuration D, the four-mode theory predicted higher speeds than the two-mode theory and was higher than experiment (or unconservative). For configuration D, the ratio of yaw stiffness to pitch stiffness was approximately 9:1. However, if the flexibility of the nacelle mounting beam, which was not considered in the analysis, were taken into account this ratio would be reduced somewhat; this may possibly account for the measured flutter speeds being somewhat lower than the predicted flutter speeds.

The Effect of Wing Aerodynamics

The effect of wing aerodynamics has been considered by omitting the wing aerodynamic terms, equation (B39), in a four-mode analysis for configuration C. The resulting flutter characteristics are compared with the two-degree-of-freedom calculations and four-degree-of-freedom calculations including wing aerodynamics in figure 14 for three propeller blade angles. The asymptotes (taken from fig. 15) which the coupled frequencies approach for large values of $\Omega/\bar{\omega}$ (with no wing or propeller aerodynamics) are included for comparison. These asymptotes represent boundaries which the coupled frequencies cannot cross (see appendix C). For the 25° blade angle, which is for large values of Ω/ω_θ, and beyond the region of high coupling, there is little difference among the calculated trends. However, for the other blade angles, two flutter solutions were obtained when wing aerodynamics were omitted. These two solutions were obtained in the region of high coupling, as indicated by the approach of two coupled frequencies to one another. However, when wing aerodynamics are included (fig. 14), only one of the flutter solutions is obtained. Thus, it is indicated that the inclusion of wing aerodynamics is quite important for cases that involve large coupling of wing and propeller motion; the omission of wing aerodynamics could lead to an unnecessarily conservative flutter speed.

CONCLUSIONS

Propeller whirl flutter boundaries were measured for a single power plant mounted on a cantilevered semispan wing for several configurations differing in power-plant parameters. An uncoupled-mode analysis of the system was made employing the following four degrees of freedom: wing bending, wing torsion, power-plant pitch, and power-plant yaw. Comparisons of experimental data, results of the four-mode analysis, and the results of an analysis including only power-plant freedoms indicate the following conclusions:

1. The effect of the wing on the whirl flutter boundary can be large depending on the system parameters. These effects were generally stabilizing for the configurations considered.

2. The four-mode analysis generally gave better results than the two-mode analysis, but only gave fair agreement in some cases.

3. In cases of large coupling between the wing and the propeller whirl modes, the inclusion of wing aerodynamics in the analysis can have large stabilizing effects.

Langley Research Center,
National Aeronautics and Space Administration,
Langley Station, Hampton, Va., April 28, 1964.

APPENDIX A

SYMBOLS

A_{ij} flutter determinant element (see eq. (B42))

a nondimensional distance from wing midchord to elastic axis, measured perpendicular to elastic axis, positive rearward, fraction of semichord b

a_c nondimensional distance from wing midchord to local aerodynamic center (for steady flow), measured perpendicular to elastic axis, positive rearward, fraction of semichord b

$(ab)_P$ distance from wing midchord to elastic axis at propeller station, positive rearward, ft

B ratio of wing local semichord to reference semichord, measured perpendicular to elastic axis, b/b_r

b wing semichord, measured perpendicular to elastic axis, ft

b_r wing reference semichord, 0.6344 ft

C_m propeller pitching-moment coefficient, $\frac{M_{Y,P}}{\rho V^2 S' R}$

C_n propeller yawing-moment coefficient, $\frac{M_{Z,P}}{\rho V^2 S' R}$

C_Y propeller side-force coefficient, $\frac{F_{Y,P}}{\frac{1}{2}\rho V^2 S'}$

C_Z propeller vertical-force coefficient, $\frac{F_{Z,P}}{\frac{1}{2}\rho V^2 S'}$

c_{l_α} wing local lift-curve slope for a streamwise section in steady flow, per radian

D dissipation function (see eq. (B21)); also propeller diameter, 2R, ft

EI wing bending stiffness, $lb\text{-}ft^2$

e_α	distance from wing elastic axis to plane of propeller-blade quarter-chord points at three-quarter radius, positive rearward, $e_\theta + l_\theta + (ab)_P$, ft
e_θ	distance from gimbal pitch axis to plane of propeller-blade quarter-chord points at three-quarter radius, positive rearward, ft
e_ψ	distance from gimbal yaw axis to plane of propeller-blade quarter-chord points at three-quarter radius, positive rearward, ft
F	real part of complex circulation function based on k_r
$F_{Y,P}$	propeller aerodynamic force along Y-axis, lb
$F_{Z,P}$	propeller aerodynamic force along Z-axis, lb
f	vibration frequency, cps
f_i	vibration frequency in ith mode, cps
G	imaginary part of complex circulation function based on k_r
GJ	wing torsional stiffness, lb-ft^2
g_i	structural damping coefficient for ith vibration mode
h	local vertical bending displacement of wing elastic axis, positive down, ft
h_P	vertical bending displacement h of wing elastic axis at the propeller station, ft
I_Ω	mass moment of inertia of propeller about axis of rotation, slug-ft^2
$I_{\alpha,W}$	generalized mass moment of inertia of wing about elastic axis (see eq. (B6)), slug-ft^2
$I_{\alpha,P}$	generalized mass moment of inertia of engine-propeller about elastic axis (see eq. (B12)), slug-ft^2
$I_{\alpha,WP}$	generalized total mass moment of inertia about elastic axis, $I_{\alpha,W} + I_{\alpha,P}$, slug-ft^2
$I_{\theta,P}$	generalized mass moment of inertia of engine-propeller about gimbal pitch axis (see eq. (B12)), slug-ft^2

$I_{\psi,P}$ generalized mass moment of inertia of engine-propeller about gimbal yaw axis (see eq. (B12)), slug-ft^2

$I_{\theta\alpha,P}$ generalized cross mass moment-of-inertia term (see eq. (B12)), slug-ft^2

$I_{\theta\psi}, I_{\psi\alpha}$ generalized mass moment of inertia of propeller about rotation axis (see eq. (B16)), slug-ft^2

$i = \sqrt{-1}$

i_θ mass moment of inertia of engine-propeller about gimbal pitch axis (see eq. (B13)), slug-ft^2

i_ψ mass moment of inertia of engine-propeller about gimbal yaw axis (see eq. (B13)), slug-ft^2

$i_{\alpha,W}(\eta)$ wing mass moment of inertia about elastic axis per unit length (see eq. (B7)), slug-ft

J windmilling propeller advance ratio, V/nD

K_i dimensional stiffness in ith vibration mode

k_r reduced frequency based on wing reference semichord, $b_r\omega/V$

l_θ distance from wing midchord to gimbal pitch axis, positive rearward, ft

l_ψ distance from wing midchord to gimbal yaw axis, positive rearward, ft

M_P engine-propeller generalized mass (see eq. (B12)), slugs

M_W wing generalized mass (see eq. (B6)), slugs

M_{WP} total generalized mass $M_W + M_P$, slugs

M_{ij} nondimensional generalized mass (see eq. (B27))

$M_{Y,P}$ propeller aerodynamic moment about Y-axis, ft-lb

$M_{Z,P}$ propeller aerodynamic moment about Z-axis, ft-lb

$M_\alpha(\eta)$ oscillatory wing aerodynamic moment about elastic axis per unit length, positive leading edge up, lb

m_P engine-propeller mass (see eq. (B13)), slugs

$m_P(x)$	engine-propeller mass per unit length, slugs/ft
$m_W(\eta)$	wing mass per unit length (see eq. (B7)), slugs/ft
$m_W(x,y)$	wing mass per unit area, slugs/sq ft
n	propeller rotational speed, rps
$P(\eta)$	oscillatory wing aerodynamic lift per unit length, positive down, lb/ft
Q_i	generalized force in ith vibration mode
$Q_{i,P}$	generalized propeller aerodynamic force in ith vibration mode
$Q_{i,W}$	generalized wing aerodynamic force in ith vibration mode
$Q_{ij,P}$	nondimensional generalized propeller aerodynamic force (see eq. (B36))
$Q_{ij,W}$	nondimensional generalized wing aerodynamic force (see eq. (B39))
q	propeller pitch rate, $\dot{\theta}R/V$
q_i	ith generalized coordinate (see eqs. (B4) and (B10))
$\bar{q}_i$	complex amplitude of q_i (see eq. (B24))
R	propeller radius, 0.8438 ft
r	propeller yaw rate, $\dot{\psi}R/V$
r_α	nondimensional radius of gyration about wing elastic axis, $\sqrt{\frac{i_{\alpha,W}(\eta)}{m_W(\eta)b^2}}$
S'	propeller disk area, πR^2, sq ft
$S_{\alpha,P}$	engine-propeller generalized mass unbalance about elastic axis (see eq. (B12)), slug-ft
$S_{\alpha,W}$	wing generalized mass unbalance about elastic axis (see eq. (B6)), slug-ft
$S_{\alpha,WP}$	total generalized mass unbalance about elastic axis, $S_{\alpha,W} + S_{\alpha,P}$, slug-ft

$S_{\theta,P}$	engine-propeller generalized mass unbalance about pitch axis (see eq. (B12)), slug-ft
s	wing semispan, ft
s_{θ}	engine-propeller mass unbalance about pitch axis (see eq. (B13)), slug-ft
$s_{\alpha,W}(\eta)$	wing mass unbalance about elastic axis per unit length (see eq. (B7)), slugs
T	kinetic energy, ft-lb
T_P	kinetic energy of engine-propeller system (see eq. (B8)), ft-lb
T_W	kinetic energy of wing (see eq. (B5)), ft-lb
T_{Ω}	kinetic energy of propeller rotation, including gyroscopic precession energy (see eq. (B14)), ft-lb
t	time, sec
U	potential energy, ft-lb
V	free-stream velocity, ft/sec
X,Y,Z	coordinate axis system (see figs. 10 and 16)
x,y,z	coordinate distances in X,Y,Z coordinate system, ft
x_{α}	nondimensional distance from wing elastic axis to local center of gravity, measured perpendicular to elastic axis, positive rearward, fraction of semichord b
y_P	lateral displacement of mass element of engine-propeller system, positive right, ft
z_P	vertical displacement of mass element of engine-propeller system, positive down, ft
z_W	vertical displacement of mass element of wing, positive down, ft
α	local wing angle of attack, positive leading edge up, radians
α_P	wing angle of attack α at propeller station, radians
$\beta_{0.75R}$	propeller blade angle at three-quarter propeller radius, deg
δ_{q_i}	virtual displacement in ith generalized coordinate

δW	virtual work, ft-lb
ζ_i	viscous-damping coefficient, ratio of viscous damping to critical damping for ith vibration mode
$\bar{\zeta}$	average viscous-damping coefficient, $\frac{\zeta_\theta + \zeta_\psi}{2}\frac{\rho_o}{\rho}$
η	nondimensional spanwise variable, fraction of semispan s
θ	pitch angle of propeller-shaft axis about gimbal axis, measured from wing chord line at propeller station, positive propeller up, radians
$\bar{\theta}$	effective engine-propeller pitch angle, measured from relative wind direction (see eq. (B33)), radians
κ_P	density-inertia ratio, $\frac{\pi\rho R^3 b_r^2}{I_{\theta,P}}$
Λ	sweep angle of wing elastic axis, deg
λ	frequency ratio, ω_θ/ω
ρ	air density, slugs/cu ft
ρ_o	nominal air density, 0.0022 slug/cu ft
φ_i	vibration mode shape in ith mode
$\varphi_{i,P}$	vibration mode shape in ith wing mode at propeller station
ψ	yaw angle of propeller-shaft axis, radians
$\bar{\psi}$	effective engine-propeller yaw angle, measured from relative wind direction (see eq. (B33)), radians
Ω	propeller rotational speed, $2\pi n$, radians/sec
ω	vibration frequency, radians/sec
ω_i	vibration frequency of ith vibration mode, radians/sec
$\bar{\omega}$	average wind-off power-plant vibration frequency, $\frac{\omega_\theta + \omega_\psi}{2}$, radians/sec

Subscripts:

f	condition at flutter
i,j	modal designation; i,j = θ, ψ, h, or α

Partial derivatives are denoted by double subscripts; for example:

$C_{m_\theta} = \frac{\partial C_m}{\partial \theta}$, $C_{m_q} = \frac{\partial C_m}{\partial q}$, and so forth.

Dots over symbols indicate derivatives with respect to time.

APPENDIX B

ANALYSIS

The analytical model considered here is pictured in figures 10 and 16. The system treated has four degrees of freedom: pitch and yaw of a single rigid engine-propeller system and wing bending and torsion. A modal-type analysis is employed to obtain stability boundaries for the system. The two elastic modes of the wing are described as bending and twisting about a straight, unswept elastic axis. Propeller and wing aerodynamic forces are included; however, the aerodynamic interference effects between the wing and propeller and the nacelle aerodynamic forces are neglected.

Equations of Motion

A Lagrangian formulation of the equations of motion is employed in which deflections in the four uncoupled vibration modes serve as generalized coordinates.

Kinetic energy.- The total kinetic energy of the system is given by

$$T = T_W + T_P + T_\Omega \tag{B1}$$

where T_W represents the contribution of the wing and rigid power-plant supporting structure; T_P represents the contribution of the flexibly mounted, nonrotating propeller-engine system; T_Ω is the energy of the rotating propeller, including the kinetic energy of gyroscopic precession.

The kinetic energy of the wing is

$$T_W = \frac{1}{2} \int\int_{Wing} m_W(x,y) \dot{z}_W^2 \, dx \, dy \tag{B2}$$

where, for bending of and twisting about an elastic axis,

$$z(x,y,t) = h + (x - ab)\alpha \tag{B3}$$

The bending h and torsion α deflections are given in terms of mode shapes and generalized coordinates by

$$\left.\begin{aligned} h(y,t) &= \varphi_h(y)q_h(t) \\ \alpha(y,t) &= \varphi_\alpha(y)q_\alpha(t) \end{aligned}\right\} \tag{B4}$$

Substituting the expressions in equations (B3) and (B4) into equation (B2) leads to the result

$$T_W = \frac{1}{2} M_W \dot{q}_h^2 + S_{\alpha,W}\dot{q}_h\dot{q}_\alpha + \frac{1}{2} I_{\alpha,W}\dot{q}_\alpha^2 \tag{B5}$$

where

$$\left.\begin{aligned} M_W &= s \int_0^1 m_W(\eta)\varphi_h^2 \, d\eta \\ S_{\alpha,W} &= s \int_0^1 s_{\alpha,W}(\eta)\varphi_h\varphi_\alpha \, d\eta \\ I_{\alpha,W} &= s \int_0^1 i_{\alpha,W}(\eta)\varphi_\alpha^2 \, d\eta \end{aligned}\right\} \tag{B6}$$

are generalized mass parameters and

$$\left.\begin{aligned} m_W(\eta) &= \int_{\text{Chord}} m_W(x,y)dx \\ s_{\alpha,W}(\eta) &= \int_{\text{Chord}} m_W(x,y)(x - ab)dx \\ i_{\alpha,W}(\eta) &= \int_{\text{Chord}} m_W(x,y)(x - ab)^2 \, dx \end{aligned}\right\} \tag{B7}$$

are wing-section mass parameters.

The kinetic energy of the nonrotating propeller is

$$T_P = \frac{1}{2} \int m_P(x)\left(\dot{z}_P^2 + \dot{y}_P^2\right)dx \tag{B8}$$

where the mass of the system is assumed to be concentrated along the propeller axis and the integration is taken over the pivoting system, and where

$$\left.\begin{aligned} z_P(x,t) &= h_P + (x - ab)\alpha_P + \left(x - l_\theta\right)\theta \\ y_P(x,t) &= -\left(x - l_\psi\right)\psi \end{aligned}\right\} \tag{B9}$$

The pitch and yaw deflections are given in terms of generalized coordinates by

$$\left.\begin{aligned} \theta(t) &= \varphi_\theta q_\theta(t) \\ \psi(t) &= \varphi_\psi q_\psi(t) \end{aligned}\right\} \tag{B10}$$

Substituting these results into equation (B8) leads to the result

$$T_P = \frac{1}{2} M_P \dot{q}_h^2 + S_{\alpha,P}\dot{q}_h\dot{q}_\alpha + \frac{1}{2} I_{\alpha,P}\dot{q}_\alpha^2 + S_{\theta,P}\dot{q}_\theta\dot{q}_h + I_{\theta\alpha,P}\dot{q}_\theta\dot{q}_\alpha + \frac{1}{2} I_{\theta,P}\dot{q}_\theta^2 + \frac{1}{2} I_{\psi,P}\dot{q}_\psi^2 \tag{B11}$$

where

$$\left.\begin{aligned} M_P &= m_P\varphi_{h,P}^2 \\ S_{\alpha,P} &= \left\{ s_\theta + \left[l_\theta - (ab)_P\right] m_P \right\} \varphi_{h,P}\varphi_{\alpha,P} \\ I_{\alpha,P} &= \left\{ i_\theta + 2\left[l_\theta - (ab)_P\right] s_\theta + \left[l_\theta - (ab)_P\right]^2 m_P \right\} \varphi_{\alpha,P}^2 \\ S_{\theta,P} &= s_\theta\varphi_\theta\varphi_{h,P} \\ I_{\theta\alpha,P} &= \left\{ i_\theta + \left[l_\theta - (ab)_P\right] s_\theta \right\} \varphi_\theta\varphi_{\alpha,P} \\ I_{\theta,P} &= i_\theta\varphi_\theta^2 \\ I_{\psi,P} &= i_\psi\varphi_\psi^2 \end{aligned}\right\} \tag{B12}$$

are generalized mass parameters and

$$\left.\begin{aligned} m_P &= \int m_P(x)\,dx \\ s_\theta &= \int m_P(x)\left(x - l_\theta\right)dx \\ i_\theta &= \int m_P(x)\left(x - l_\theta\right)^2 dx \\ i_\psi &= \int m_P(x)\left(x - l_\psi\right)^2 dx \end{aligned}\right\} \tag{B13}$$

are engine-propeller mass parameters. The integrations are carried out over the pivoting engine-propeller system.

The kinetic energy of the rotating propeller is given by an obvious extension of the result in reference 1 as

$$T_\Omega = \frac{1}{2} I_\Omega\left[\Omega^2 + 2\Omega\left(\dot\theta + \dot\alpha_P\right)\psi\right] \tag{B14}$$

In terms of the generalized coordinates in equations (B4) and (B10) equation (B14) becomes

$$T_\Omega = \frac{1}{2} I_\Omega \Omega^2 + I_{\theta\psi}{}^{\Omega}\dot q_\theta q_\psi + I_{\psi\alpha}{}^{\Omega} q_\psi \dot q_\alpha \tag{B15}$$

where I_Ω is the mass moment of inertia of the propeller about its axis of rotation and

$$\left.\begin{aligned} I_{\theta\psi} &= I_\Omega \varphi_\theta \varphi_\psi \\ I_{\psi\alpha} &= I_\Omega \varphi_\psi \varphi_{\alpha,P} \end{aligned}\right\} \tag{B16}$$

are generalized mass parameters of the engine-propeller system.

The total kinetic energy is seen to be

$$\begin{aligned} T = {} & \frac{1}{2} I_{\theta,P}\dot q_\theta^2 + I_{\theta\psi}{}^{\Omega}\dot q_\theta q_\psi + S_{\theta,P}\dot q_\theta \dot q_h + I_{\theta\alpha,P}\dot q_\theta \dot q_\alpha + \frac{1}{2} I_{\psi,P}\dot q_\psi^2 + I_{\psi\alpha}{}^{\Omega} q_\psi \dot q_\alpha \\ & + \frac{1}{2} M_{WP}\dot q_h^2 + S_{\alpha,WP}\dot q_h \dot q_\alpha + \frac{1}{2} I_{\alpha,WP}\dot q_\alpha^2 + \frac{1}{2} I_\Omega \Omega^2 \end{aligned} \tag{B17}$$

where

$$\left.\begin{aligned} M_{WP} &= M_W + M_P \\ S_{\alpha,WP} &= S_{\alpha,W} + S_{\alpha,P} \\ I_{\alpha,WP} &= I_{\alpha,W} + I_{\alpha,P} \end{aligned}\right\} \tag{B18}$$

Potential energy.- The potential energy may be expressed in the form

$$U = \frac{1}{2} K_\theta q_\theta^2 + \frac{1}{2} K_\psi q_\psi^2 + \frac{1}{2} K_h q_h^2 + \frac{1}{2} K_\alpha q_\alpha^2 \tag{B19}$$

where K is generalized stiffness. In terms of uncoupled frequencies and generalized masses the potential energy is expressed as

$$U = \frac{1}{2} I_{\theta,P} \omega_\theta^2 q_\theta^2 + \frac{1}{2} I_{\psi,P} \omega_\psi^2 q_\psi^2 + \frac{1}{2} M_{WP} \omega_h^2 q_h^2 + \frac{1}{2} I_{\alpha,WP} \omega_\alpha^2 q_\alpha^2 \tag{B20}$$

Dissipation function.- The structural damping concept, in which a dissipative force proportional to displacement is employed, will be used in the derivation herein. For such damping, the dissipation function is

$$D = \frac{1}{2} I_{\theta,P} g_\theta \frac{\omega_\theta^2}{\omega} \dot{q}_\theta^2 + \frac{1}{2} I_{\psi,P} g_\psi \frac{\omega_\psi^2}{\omega} \dot{q}_\psi^2 + \frac{1}{2} M_{WP} g_h \frac{\omega_h^2}{\omega} \dot{q}_h^2 + \frac{1}{2} I_{\alpha,WP} g_\alpha \frac{\omega_\alpha^2}{\omega} \dot{q}_\alpha^2 \tag{B21}$$

where ω is the frequency of vibration of the system and g is the structural damping coefficient.

Lagrange's equations.- The equations of motion of the system are obtained from Lagrange's equation

$$\frac{d}{dt}\left(\frac{\partial T}{\partial \dot{q}_i}\right) - \frac{\partial T}{\partial q_i} + \frac{\partial U}{\partial q_i} + \frac{\partial D}{\partial \dot{q}_i} = Q_i \tag{B22}$$

where $i = \theta$, ψ, h, or α. Substituting the expressions from equations (B17), (B20), and (B21) into equation (B22) and performing the indicated operations yields the equations of motion

$$
\left.
\begin{aligned}
&I_{\theta,P}\left(\ddot{q}_\theta + g_\theta \frac{\omega_\theta^2}{\omega}\dot{q}_\theta + \omega_\theta^2 q_\theta\right) + I_{\theta\psi}\Omega\dot{q}_\psi + S_{\theta,P}\ddot{q}_h + I_{\theta\alpha,P}\ddot{q}_\alpha = Q_\theta \\
&-I_{\theta\psi}\Omega\dot{q}_\theta + I_{\psi,P}\left(\ddot{q}_\psi + g_\psi \frac{\omega_\psi^2}{\omega}\dot{q}_\psi + \omega_\psi^2 q_\psi\right) - I_{\psi\alpha}\Omega\dot{q}_\alpha = Q_\psi \\
&S_{\theta,P}\ddot{q}_\theta + M_{WP}\left(\ddot{q}_h + g_h \frac{\omega_h^2}{\omega}\dot{q}_h + \omega_h^2 q_h\right) + S_{\alpha,WP}\ddot{q}_\alpha = Q_h \\
&I_{\theta\alpha,P}\ddot{q}_\theta + I_{\psi\alpha}\Omega\dot{q}_\psi + S_{\alpha,WP}\ddot{q}_h + I_{\alpha,WP}\left(\ddot{q}_\alpha + g_\alpha \frac{\omega_\alpha^2}{\omega}\dot{q}_\alpha + \omega_\alpha^2 q_\alpha\right) = Q_\alpha
\end{aligned}
\right\} \qquad \text{(B23)}
$$

Assume simple harmonic motion with

$$
\left.
\begin{aligned}
q_\theta &= \bar{q}_\theta e^{i\omega t} \\
q_\psi &= \bar{q}_\psi e^{i\omega t} \\
q_h &= \bar{q}_h e^{i\omega t} \\
q_\alpha &= \bar{q}_\alpha e^{i\omega t}
\end{aligned}
\right\} \qquad \text{(B24)}
$$

where $\bar{q}_\theta$, etc., are complex amplitudes of motion. Making these substitutions in equation (B23) and dividing the θ, ψ, and α equations by $-I_{\theta,P}\omega^2 e^{i\omega t}$ and the h equation by $-\frac{1}{R} I_{\theta,P}\omega^2 e^{i\omega t}$ (R being the propeller radius) yields the nondimensional equations of motion

$$
\left.
\begin{aligned}
&\left[1 - \lambda^2\left(1 + ig_\theta\right)\right]\bar{q}_\theta - iM_{\theta\psi}\frac{\pi}{Jk_r}\bar{q}_\psi + M_{\theta h}\frac{\bar{q}_h}{R} + M_{\theta\alpha}\bar{q}_\alpha = -\frac{Q_\theta}{I_{\theta,P}\omega^2} e^{-i\omega t} \\
&iM_{\theta\psi}\frac{\pi}{Jk_r}\bar{q}_\theta + M_{\psi\psi}\left[1 - \lambda^2\left(\frac{\omega_\psi}{\omega_\theta}\right)^2\left(1 + ig_\psi\right)\right]\bar{q}_\psi + iM_{\psi\alpha}\frac{\pi}{Jk_r}\bar{q}_\alpha = -\frac{Q_\psi}{I_{\theta,P}\omega^2} e^{-i\omega t} \\
&M_{\theta h}\bar{q}_\theta + M_{hh}\left[1 - \lambda^2\left(\frac{\omega_h}{\omega_\theta}\right)^2\left(1 + ig_h\right)\right]\frac{\bar{q}_h}{R} + M_{h\alpha}\bar{q}_\alpha = -\frac{RQ_h}{I_{\theta,P}\omega^2} e^{-i\omega t} \\
&M_{\theta\alpha}\bar{q}_\theta - iM_{\psi\alpha}\frac{\pi}{Jk_r}\bar{q}_\psi + M_{h\alpha}\frac{\bar{q}_h}{R} + M_{\alpha\alpha}\left[1 - \lambda^2\left(\frac{\omega_\alpha}{\omega_\theta}\right)^2\left(1 + ig_\alpha\right)\right]\bar{q}_\alpha = -\frac{Q_\alpha}{I_{\theta,P}\omega^2} e^{-i\omega t}
\end{aligned}
\right\} \qquad \text{(B25)}
$$

where

$$\left.\begin{aligned} \lambda &= \frac{\omega_\theta}{\omega} \\ J &= \frac{\pi V}{\Omega R} \\ k_r &= \frac{b_r \omega}{V} \end{aligned}\right\} \tag{B26}$$

are nondimensional frequency parameters, b_r is the wing reference semichord, and

$$\left.\begin{aligned} M_{\theta\psi} &= \left(\frac{I_{\theta\psi}}{I_{\theta,P}}\right)\left(\frac{b_r}{R}\right) \\ M_{\theta h} &= \frac{S_{\theta,P}R}{I_{\theta,P}} \\ M_{\theta\alpha} &= \frac{I_{\theta\alpha,P}}{I_{\theta,P}} \\ M_{\psi\psi} &= \frac{I_{\psi,P}}{I_{\theta,P}} \\ M_{\psi\alpha} &= \left(\frac{I_{\psi\alpha}}{I_{\theta,P}}\right)\left(\frac{b_r}{R}\right) \\ M_{hh} &= \frac{M_{WP}R^2}{I_{\theta,P}} \\ M_{h\alpha} &= \frac{S_{\alpha,WP}R}{I_{\theta,P}} \\ M_{\alpha\alpha} &= \frac{I_{\alpha,WP}}{I_{\theta,P}} \end{aligned}\right\} \tag{B27}$$

are nondimensional generalized masses.

Generalized Aerodynamic Forces

The aerodynamic forces acting on the propeller are expressed in terms of propeller stability derivatives as was done in references 1, 2, and 8. The modified-strip analysis method of reference 11 is employed to represent the wing aerodynamic forces. The directions of the aerodynamic forces and moments are shown in figure 16.

Virtual work.- The expression for the work done on the system by virtual displacements of the coordinates is

$$\delta W = Q_\theta \delta q_\theta + Q_\psi \delta q_\psi + Q_h \delta q_h + Q_\alpha \delta q_\alpha \tag{B28}$$

where the generalized forces have the following representations in terms of propeller and wing aerodynamics

$$\left.\begin{aligned} Q_\theta &= Q_{\theta,P} \\ Q_\psi &= Q_{\psi,P} \\ Q_h &= Q_{h,P} + Q_{h,W} \\ Q_\alpha &= Q_{\alpha,P} + Q_{\alpha,W} \end{aligned}\right\} \tag{B29}$$

Propeller aerodynamic forces.- The aerodynamic forces acting on the propeller are (see fig. 16)

$$\left.\begin{aligned} Q_{\theta,P} &= \left(M_{Y,P} + e_\theta F_{Z,P}\right)\varphi_\theta \\ Q_{\psi,P} &= \left(M_{Z,P} - e_\psi F_{Y,P}\right)\varphi_\psi \\ Q_{h,P} &= F_{Z,P}\varphi_{h,P} \\ Q_{\alpha,P} &= \left(M_{Y,P} + e_\alpha F_{Z,P}\right)\varphi_{\alpha,P} \end{aligned}\right\} \tag{B30}$$

where

$$e_\alpha = e_\theta + l_\theta + (ab)_P \tag{B31}$$

As in references 1 and 8, $M_{Y,P}$ and $M_{Z,P}$ are moments about the Y- and Z-axes in the propeller plane and $F_{Y,P}$ and $F_{Z,P}$ are forces acting in the Y and Z directions on the propeller axis in the propeller plane. These forces and moments may be expressed in terms of propeller stability derivatives as

$$\left.\begin{aligned}
F_{Z,P} &= \frac{1}{2}\rho V^2 S'\left(C_{Z_\theta}\bar{\theta} + C_{Z_q}\frac{R}{V}\dot{\bar{\theta}} + C_{Z_\psi}\bar{\psi} + C_{Z_r}\frac{R}{V}\dot{\bar{\psi}}\right) \\
F_{Y,P} &= \frac{1}{2}\rho V^2 S'\left(C_{Y_\theta}\bar{\theta} + C_{Y_q}\frac{R}{V}\dot{\bar{\theta}} + C_{Y_\psi}\bar{\psi} + C_{Y_r}\frac{R}{V}\dot{\bar{\psi}}\right) \\
M_{Y,P} &= \rho V^2 S' R\left(C_{m_\theta}\bar{\theta} + C_{m_q}\frac{R}{V}\dot{\bar{\theta}} + C_{m_\psi}\bar{\psi} + C_{m_r}\frac{R}{V}\dot{\bar{\psi}}\right) \\
M_{Z,P} &= \rho V^2 S' R\left(C_{n_\theta}\bar{\theta} + C_{n_q}\frac{R}{V}\dot{\bar{\theta}} + C_{n_\psi}\bar{\psi} + C_{n_r}\frac{R}{V}\dot{\bar{\psi}}\right)
\end{aligned}\right\} \tag{B32}$$

where $S' = \pi R^2$, and

$$\left.\begin{aligned}
\bar{\theta} &= \theta + \alpha_P + \frac{e_\theta}{V}\dot{\theta} + \frac{e_\alpha}{V}\dot{\alpha}_P + \frac{1}{V}\dot{h}_P \\
\bar{\psi} &= \psi + \frac{e_\psi}{V}\dot{\psi}
\end{aligned}\right\} \tag{B33}$$

are pitch and yaw angles with respect to the relative wind direction. Notice that in equation (B32) all possible force and moment derivatives that depend on angle and angular rate are included; angular acceleration derivatives (which account for virtual mass effects) have been neglected, as in reference 1. The substitution of equation (B33) into equation (B32), the use of generalized coordinates (eqs. (B4) and (B10)), and the assumption of harmonic motion (eq. (B24)) lead to the final expressions for the nondimensional propeller aerodynamic forces

$$\left.\begin{aligned}
\frac{Q_{\theta,P}}{I_{\theta,P}\omega^2}e^{-i\omega t} &= \frac{\kappa_P}{k_r^2}\left(Q_{\theta\theta,P}\bar{q}_\theta + Q_{\theta\psi,P}\bar{q}_\psi + Q_{\theta h,P}\frac{\bar{q}_h}{R} + Q_{\theta\alpha,P}\bar{q}_\alpha\right) \\
\frac{Q_{\psi,P}}{I_{\theta,P}\omega^2}e^{-i\omega t} &= \frac{\kappa_P}{k_r^2}\left(Q_{\psi\theta,P}\bar{q}_\theta + Q_{\psi\psi,P}\bar{q}_\psi + Q_{\psi h,P}\frac{\bar{q}_h}{R} + Q_{\psi\alpha,P}\bar{q}_\alpha\right) \\
\frac{RQ_{h,P}}{I_{\theta,P}\omega^2}e^{-i\omega t} &= \frac{\kappa_P}{k_r^2}\left(Q_{h\theta,P}\bar{q}_\theta + Q_{h\psi,P}\bar{q}_\psi + Q_{hh,P}\frac{\bar{q}_h}{R} + Q_{h\alpha,P}\bar{q}_\alpha\right) \\
\frac{Q_{\alpha,P}}{I_{\theta,P}\omega^2}e^{-i\omega t} &= \frac{\kappa_P}{k_r^2}\left(Q_{\alpha\theta,P}\bar{q}_\theta + Q_{\alpha\psi,P}\bar{q}_\psi + Q_{\alpha h,P}\frac{\bar{q}_h}{R} + Q_{\alpha\alpha,P}\bar{q}_\alpha\right)
\end{aligned}\right\} \tag{B34}$$

where

$$\kappa_P = \frac{\pi\rho R^3 b_r^2}{I_{\theta,P}} \tag{B35}$$

is an inertia ratio parameter and

$$\left.\begin{aligned}
Q_{\theta\theta,P} &= \left[\left(1 + ik_r \frac{e_\theta}{b_r}\right)\left(C_{m_\theta} + \frac{e_\theta}{D} C_{Z_\theta}\right) + \left(ik_r \frac{R}{b_r} - k_r^2 \frac{e_\theta R}{b_r^2}\right)\left(C_{m_q} + \frac{e_\theta}{D} C_{Z_q}\right)\right]\varphi_\theta^2 \\
Q_{\theta\psi,P} &= \left[\left(1 + ik_r \frac{e_\psi}{b_r}\right)\left(C_{m_\psi} + \frac{e_\theta}{D} C_{Z_\psi}\right) + \left(ik_r \frac{R}{b_r} - k_r^2 \frac{e_\psi R}{b_r^2}\right)\left(C_{m_r} + \frac{e_\theta}{D} C_{Z_r}\right)\right]\varphi_\theta\varphi_\psi \\
Q_{\theta h,P} &= \left[ik_r \frac{R}{b_r}\left(C_{m_\theta} + \frac{e_\theta}{D} C_{Z_\theta}\right) - k_r^2 \frac{R^2}{b_r^2}\left(C_{m_q} + \frac{e_\theta}{D} C_{Z_q}\right)\right]\varphi_\theta\varphi_{h,P} \\
Q_{\theta\alpha,P} &= \left[\left(1 + ik_r \frac{e_\alpha}{b_r}\right)\left(C_{m_\theta} + \frac{e_\theta}{D} C_{Z_\theta}\right) + \left(ik_r \frac{R}{b_r} - k_r^2 \frac{e_\alpha R}{b_r^2}\right)\left(C_{m_q} + \frac{e_\theta}{D} C_{Z_q}\right)\right]\varphi_\theta\varphi_{\alpha,P} \\
Q_{\psi\theta,P} &= \left[\left(1 + ik_r \frac{e_\theta}{b_r}\right)\left(C_{n_\theta} - \frac{e_\psi}{D} C_{Y_\theta}\right) + \left(ik_r \frac{R}{b_r} - k_r^2 \frac{e_\theta R}{b_r^2}\right)\left(C_{n_q} - \frac{e_\psi}{D} C_{Y_q}\right)\right]\varphi_\psi\varphi_\theta \\
Q_{\psi\psi,P} &= \left[\left(1 + ik_r \frac{e_\psi}{b_r}\right)\left(C_{n_\psi} - \frac{e_\psi}{D} C_{Y_\psi}\right) + \left(ik_r \frac{R}{b_r} - k_r^2 \frac{e_\psi R}{b_r^2}\right)\left(C_{n_r} - \frac{e_\psi}{D} C_{Y_r}\right)\right]\varphi_\psi^2 \\
Q_{\psi h,P} &= \left[ik_r \frac{R}{b_r}\left(C_{n_\theta} - \frac{e_\psi}{D} C_{Y_\theta}\right) - k_r^2 \frac{R^2}{b_r^2}\left(C_{n_q} - \frac{e_\psi}{D} C_{Y_q}\right)\right]\varphi_\psi\varphi_{h,P} \\
Q_{\psi\alpha,P} &= \left[\left(1 + ik_r \frac{e_\alpha}{b_r}\right)\left(C_{n_\theta} - \frac{e_\psi}{D} C_{Y_\theta}\right) + \left(ik_r \frac{R}{b_r} - k_r^2 \frac{e_\alpha R}{b_r^2}\right)\left(C_{n_q} - \frac{e_\psi}{D} C_{Y_q}\right)\right]\varphi_\psi\varphi_{\alpha,P} \\
Q_{h\theta,P} &= \tfrac{1}{2}\left[\left(1 + ik_r \frac{e_\theta}{b_r}\right)C_{Z_\theta} + \left(ik_r \frac{R}{b_r} - k_r^2 \frac{e_\theta R}{b_r^2}\right)C_{Z_q}\right]\varphi_{h,P}\varphi_\theta \\
Q_{h\psi,P} &= \tfrac{1}{2}\left[\left(1 + ik_r \frac{e_\psi}{b_r}\right)C_{Z_\psi} + \left(ik_r \frac{R}{b_r} - k_r^2 \frac{e_\psi R}{b_r^2}\right)C_{Z_r}\right]\varphi_{h,P}\varphi_\psi \\
Q_{hh,P} &= \tfrac{1}{2}\left(ik_r \frac{R}{b_r} C_{Z_\theta} - k_r^2 \frac{R^2}{b_r^2} C_{Z_q}\right)\varphi_{h,P}^2 \\
Q_{h\alpha,P} &= \tfrac{1}{2}\left[\left(1 + ik_r \frac{e_\alpha}{b_r}\right)C_{Z_\theta} + \left(ik_r \frac{R}{b_r} - k_r^2 \frac{e_\alpha R}{b_r^2}\right)C_{Z_q}\right]\varphi_{h,P}\varphi_{\alpha,P} \\
Q_{\alpha\theta,P} &= \left[\left(1 + ik_r \frac{e_\theta}{b_r}\right)\left(C_{m_\theta} + \frac{e_\alpha}{D} C_{Z_\theta}\right) + \left(ik_r \frac{R}{b_r} - k_r^2 \frac{e_\theta R}{b_r^2}\right)\left(C_{m_q} + \frac{e_\alpha}{D} C_{Z_q}\right)\right]\varphi_{\alpha,P}\varphi_\theta \\
Q_{\alpha\psi,P} &= \left[\left(1 + ik_r \frac{e_\psi}{b_r}\right)\left(C_{m_\psi} + \frac{e_\alpha}{D} C_{Z_\psi}\right) + \left(ik_r \frac{R}{b_r} - k_r^2 \frac{e_\psi R}{b_r^2}\right)\left(C_{m_r} + \frac{e_\alpha}{D} C_{Z_r}\right)\right]\varphi_{\alpha,P}\varphi_\psi \\
Q_{\alpha h,P} &= \left[ik_r \frac{R}{b_r}\left(C_{m_\theta} + \frac{e_\alpha}{D} C_{Z_\theta}\right) - k_r^2 \frac{R^2}{b_r^2}\left(C_{m_q} + \frac{e_\alpha}{D} C_{Z_q}\right)\right]\varphi_{\alpha,P}\varphi_{h,P} \\
Q_{\alpha\alpha,P} &= \left[\left(1 + ik_r \frac{e_\alpha}{b_r}\right)\left(C_{m_\theta} + \frac{e_\alpha}{D} C_{Z_\theta}\right) + \left(ik_r \frac{R}{b_r} - k_r^2 \frac{e_\alpha R}{b_r^2}\right)\left(C_{m_q} + \frac{e_\alpha}{D} C_{Z_q}\right)\right]\varphi_{\alpha,P}^2
\end{aligned}\right\} \tag{B36}$$

Wing aerodynamic forces.- The aerodynamic forces acting on the wing (introduced in eq. (B29)) are given in general as

$$\left.\begin{aligned} Q_{h,W} &= s \int_0^1 P(\eta)\varphi_h \, d\eta \\ Q_{\alpha,W} &= s \int_0^1 M_\alpha(\eta)\varphi_\alpha \, d\eta \end{aligned}\right\} \tag{B37}$$

where $P(\eta)$ is the wing-section lift force and $M_\alpha(\eta)$ is the section pitching moment about the elastic axis. Any suitable unsteady aerodynamic theory may be used to evaluate these expressions. In this report, the modified-strip analysis method of reference 11 is employed as follows:

$$\left.\begin{aligned} \frac{RQ_{h,W}}{I_{\theta,P}\omega^2} e^{-i\omega t} &= \frac{\kappa_P}{k_r^2}\left(Q_{hh,W}\frac{\bar{q}_h}{R} + Q_{h\alpha,W}\bar{q}_\alpha\right) \\ \frac{Q_{\alpha,W}}{I_{\theta,P}\omega^2} e^{-i\omega t} &= \frac{\kappa_P}{k_r^2}\left(Q_{\alpha h,W}\frac{\bar{q}_h}{R} + Q_{\alpha\alpha,W}\bar{q}_\alpha\right) \end{aligned}\right\} \tag{B38}$$

where, for an unswept elastic axis,

$$\left.\begin{aligned} Q_{hh,W} &= \left[\left(②\right) + \frac{G}{\pi k_r}\left(③\right)\right) - i\,\frac{F}{\pi k_r}\left(③\right)\right]\frac{s}{R}k_r^2 \\ Q_{h\alpha,W} &= \left[\left(-⑬ - \frac{F}{\pi k_r^2}⑪ + \frac{G}{\pi k_r}⑫\right) - i\left(\frac{1}{k_r}⑭ + \frac{G}{\pi k_r^2}⑪ + \frac{F}{\pi k_r}⑫\right)\right]\frac{sb_r}{R^2}k_r^2 \\ Q_{\alpha h,W} &= \left[\left(-⑬ - \frac{G}{\pi k_r}⑰\right) + i\,\frac{F}{\pi k_r}⑰\right]\frac{sb_r}{R^2}k_r^2 \\ Q_{\alpha\alpha,W} &= \left[\left(㉒ + \frac{F}{\pi k_r^2}㉑ - \frac{G}{\pi k_r}㉓\right) - i\left(\frac{1}{k_r}㉔ - \frac{G}{\pi k_r^2}㉑ - \frac{F}{\pi k_r}㉓\right)\right]\frac{sb_r^2}{R^3}k_r^2 \end{aligned}\right\} \tag{B39}$$

The circulation functions for unsteady flow, F and G, depend, in general, on k_r and Mach number. The circled numbers are the integrals given in appendix A of reference 11. They are, in the present notation,

$$
\begin{aligned}
\textcircled{2} &= \int_0^1 B^2 \varphi_h^2 \, d\eta \\
\textcircled{3} &= \int_0^1 c_{l_\alpha} B \varphi_h^2 \, d\eta \\
\textcircled{11} &= \int_0^1 c_{l_\alpha} B \varphi_h \varphi_\alpha \, d\eta \\
\textcircled{12} &= \int_0^1 c_{l_\alpha} B^2 \left(\frac{c_{l_\alpha}}{2\pi} + a_c - a \right) \varphi_h \varphi_\alpha \, d\eta \\
\textcircled{13} &= \int_0^1 B^3 a \varphi_h \varphi_\alpha \, d\eta \\
\textcircled{14} &= \int_0^1 B^2 \varphi_h \varphi_\alpha \, d\eta \\
\textcircled{17} &= \int_0^1 c_{l_\alpha} B^2 (a - a_c) \varphi_h \varphi_\alpha \, d\eta \\
\textcircled{21} &= \int_0^1 c_{l_\alpha} B^2 (a - a_c) \varphi_\alpha^2 \, d\eta \\
\textcircled{22} &= \int_0^1 B^4 \left(\frac{1}{8} + a^2 \right) \varphi_\alpha^2 \, d\eta \\
\textcircled{23} &= \int_0^1 c_{l_\alpha} B^3 \left(\frac{c_{l_\alpha}}{2\pi} + a_c - a \right) (a - a_c) \varphi_\alpha^2 \, d\eta \\
\textcircled{24} &= \int_0^1 B^3 \left(\frac{c_{l_\alpha}}{2\pi} + a_c - a \right) \varphi_\alpha^2 \, d\eta
\end{aligned}
\qquad \text{(B40)}
$$

Flutter Determinant

Substituting equations (B34) and (B38) into equation (B25) yields the final form for the equations of motion. In matrix notation

$$\begin{bmatrix} A_{\theta\theta} & A_{\theta\psi} & A_{\theta h} & A_{\theta\alpha} \\ A_{\psi\theta} & A_{\psi\psi} & A_{\psi h} & A_{\psi\alpha} \\ A_{h\theta} & A_{h\psi} & A_{hh} & A_{h\alpha} \\ A_{\alpha\theta} & A_{\alpha\psi} & A_{\alpha h} & A_{\alpha\alpha} \end{bmatrix} \begin{Bmatrix} \bar{q}_\theta \\ \bar{q}_\psi \\ \bar{q}_h/R \\ \bar{q}_\alpha \end{Bmatrix} = 0 \tag{B41}$$

where

$$\left.\begin{aligned}
A_{\theta\theta} &= 1 - \lambda^2\left(1 + ig_\theta\right) + \frac{\kappa_P}{k_r^2} Q_{\theta\theta,P} \\
A_{\theta\psi} &= -iM_{\theta\psi} \frac{\pi}{Jk_r} + \frac{\kappa_P}{k_r^2} Q_{\theta\psi,P} \\
A_{\theta h} &= M_{\theta h} + \frac{\kappa_P}{k_r^2} Q_{\theta h,P} \\
A_{\theta\alpha} &= M_{\theta\alpha} + \frac{\kappa_P}{k_r^2} Q_{\theta\alpha,P} \\
A_{\psi\theta} &= iM_{\theta\psi} \frac{\pi}{Jk_r} + \frac{\kappa_P}{k_r^2} Q_{\psi\theta,P} \\
A_{\psi\psi} &= M_{\psi\psi}\left[1 - \lambda^2\left(\frac{\omega_\psi}{\omega_\theta}\right)^2\left(1 + i\,\frac{g_\psi}{g_\theta}\,g_\theta\right)\right] + \frac{\kappa_P}{k_r^2} Q_{\psi\psi,P} \\
A_{\psi h} &= \frac{\kappa_P}{k_r^2} Q_{\psi h,P} \\
A_{\psi\alpha} &= iM_{\psi\alpha} \frac{\pi}{Jk_r} + \frac{\kappa_P}{k_r^2} Q_{\psi\alpha,P} \\
A_{h\theta} &= M_{\theta h} + \frac{\kappa_P}{k_r^2} Q_{h\theta,P} \\
A_{h\psi} &= \frac{\kappa_P}{k_r^2} Q_{h\psi,P} \\
A_{hh} &= M_{hh}\left[1 - \lambda^2\left(\frac{\omega_h}{\omega_\theta}\right)^2\left(1 + ig_h\right)\right] + \frac{\kappa_P}{k_r^2}\left(Q_{hh,P} + Q_{hh,W}\right) \\
A_{h\alpha} &= M_{h\alpha} + \frac{\kappa_P}{k_r^2}\left(Q_{h\alpha,P} + Q_{h\alpha,W}\right) \\
A_{\alpha\theta} &= M_{\theta\alpha} + \frac{\kappa_P}{k_r^2} Q_{\alpha\theta,P} \\
A_{\alpha\psi} &= -iM_{\psi\alpha} \frac{\pi}{Jk_r} + \frac{\kappa_P}{k_r^2} Q_{\alpha\psi,P} \\
A_{\alpha h} &= M_{h\alpha} + \frac{\kappa_P}{k_r^2}\left(Q_{\alpha h,P} + Q_{\alpha h,W}\right) \\
A_{\alpha\alpha} &= M_{\alpha\alpha}\left[1 - \lambda^2\left(\frac{\omega_\alpha}{\omega_\theta}\right)^2\left(1 + ig_\alpha\right)\right] + \frac{\kappa_P}{k_r^2}\left(Q_{\alpha\alpha,P} + Q_{\alpha\alpha,W}\right)
\end{aligned}\right\} \tag{B42}$$

In order for this set of equations (eq. (B41)) to have a nontrivial solution, the determinant of the coefficient matrix must vanish. This flutter determinant is

$$\begin{vmatrix} A_{\theta\theta} & A_{\theta\psi} & A_{\theta h} & A_{\theta\alpha} \\ A_{\psi\theta} & A_{\psi\psi} & A_{\psi h} & A_{\psi\alpha} \\ A_{h\theta} & A_{h\psi} & A_{hh} & A_{h\alpha} \\ A_{\alpha\theta} & A_{\alpha\psi} & A_{\alpha h} & A_{\alpha\alpha} \end{vmatrix} = 0 \tag{B43}$$

Application of Analysis

Solution of determinant.- The flutter determinant has been programed for a high-speed electronic digital computer. In this program, for a given case, all input quantities are fixed except k_r, g_θ, and λ^2. A sequence of values of reduced frequency k_r and propeller structural damping in pitch g_θ is used. For each combination of values of k_r and g_θ the flutter determinant is expanded to give a fourth degree characteristic polynominal in λ^2. Points of neutral stability of the system are obtained for the combination of values of k_r and g_θ that makes one of the four roots of the characteristic polynominal a positive real quantity. The values of k_r, g_θ, and λ^2 at this point of neutral stability are used herein to compute the flutter frequency ratio

$$\frac{\omega}{\omega_\theta} = \frac{1}{\lambda} \tag{B44}$$

the flutter speed ratio

$$\frac{V}{R\omega_\theta} = \frac{b_r}{R}\frac{1}{\lambda}\frac{1}{k_r} \tag{B45}$$

and the equivalent viscous damping (see ref. 1) required for neutral stability

$$2\zeta_\theta = g_\theta\lambda \tag{B46}$$

Whirl flutter boundaries are known to be quite sensitive to the amount of structural damping in the system (see refs. 1, 2, and 5, for example); hence, it was not desirable to assume equal damping in all four modes of this analysis. This is the reason for the choice of the somewhat lengthy method of solution outlined. This procedure allows the wing and propeller-engine damping to be varied independently.

With the solution of the flutter determinant obtained as outlined here the elements in the square matrix in equation (B41) are completely specified. By choosing one of the four generalized coordinates, say $\bar{q}_\alpha$, arbitrarily, it is possible to solve this set of equations for the ratios of the other generalized coordinates to $\bar{q}_\alpha$. The relative magnitudes and phases of these complex amplitude ratios give some indication of the nature of the flutter mode.

Determination of input quantities.- The input quantities required to solve the flutter determinant are listed in equation (B42). These quantities were obtained as outlined in this section.

The nondimensional generalized mass parameters M_{ij} are listed in equation (B27). The required integrals were evaluated by using the measured mass properties of the model with the computed, uncoupled wing bending and torsion mode shapes (fig. 9). The propeller-engine mode shapes, φ_θ and φ_ψ, were taken as unity. The wing bending and torsion frequencies employed were those calculated for the computed modes. The engine-propeller frequencies, ω_θ and ω_ψ, were uncoupled, measured frequencies. The propeller yaw-to-pitch damping ratio, g_ψ/g_θ, was taken as unity in all cases. The wing structural damping coefficient for the first coupled mode was measured and found to be 0.005. It was assumed that the damping coefficient for both uncoupled wing modes was also this value.

As indicated in table II, there was a small variation in density among the data points. In the analysis, a nominal value of $\rho_o = 0.0022$ slug/cu ft was used.

The propeller nondimensional generalized aerodynamic forces are listed in equation (B36). For no aerodynamic interference between the wing and the propeller, the following symmetry relations between propeller stability derivatives may be assumed:

$$\left.\begin{aligned} C_{m_\theta} &= C_{n_\psi} \\ C_{Z_\theta} &= -C_{Y_\psi} \\ C_{m_q} &= C_{n_r} \\ C_{m_\psi} &= -C_{n_\theta} \\ C_{Z_\psi} &= C_{Y_\theta} \end{aligned}\right\} \qquad \text{(B47)}$$

All other propeller derivatives were neglected. The values of the static derivatives $\left(C_{m_\theta},\ C_{Z_\theta},\ C_{m_\psi},\ C_{Z_\psi}\right)$ used were measured values reported in

reference 8 for a windmilling propeller. As in this reference, the values of C_{m_q} employed were those computed by the method of reference 16. These derivatives are listed in table III for the five propeller blade angle settings used in these tests. The values of windmilling-propeller advance ratio, J, and the distances from the gimbal axes to the plane of propeller-blade quarter-chord points at three-quarter radius, e_θ and e_ψ, are also listed in table III. In all cases considered $e_\theta = e_\psi$.

The wing nondimensional generalized aerodynamic forces are given in equation (B39). The aerodynamic integrals (eq. (B40)) were evaluated numerically by using the calculated bending and torsion mode shapes. The c_{l_α} and a_c values for the exposed panel were computed from three-dimensional lifting-surface theory (kernel function method) for the planform of this model treated as a rigid wing at a steady-state angle of attack at zero Mach number. These parameters are shown in figure 17. It should be noted that these aerodynamic integrals (eq. (B40)) remain constant throughout the analysis.

APPENDIX C

EFFECT OF GYROSCOPIC COUPLING ON THE FREQUENCIES OF VIBRATION MODES

Derivation of the Frequency Equation

The effects of gyroscopic coupling on the vibration mode frequencies are examined at zero airspeed by determining the coupled vibration frequencies over a wide range of propeller rotational speed. The frequency equation for zero airspeed is obtained from the flutter determinant (eq. (B43)) by equating the generalized aerodynamic forces Q_{ij} to zero in the determinant elements (eq. (B42)) and by expanding the resulting determinant. The effect of damping on the vibrational frequencies is neglected, such that g is zero in all modes. In addition, the factor $\pi/k_r J$ in the off-diagonal mass terms, which is based on the assumption of a windmilling propeller, is put in the form $\frac{R\Omega}{b_r\omega_\theta}\lambda$. The determinant for the coupled frequencies then becomes:

$$\begin{vmatrix} 1-\lambda^2 & -iM_{\theta\psi}\frac{R\Omega}{b_r\omega_\theta}\lambda & M_{\theta h} & M_{\theta\alpha} \\ iM_{\theta\psi}\frac{R\Omega}{b_r\omega_\theta}\lambda & M_{\psi\psi}\left(1-\lambda^2\frac{\omega_\psi^2}{\omega_\theta^2}\right) & 0 & iM_{\psi\alpha}\frac{R\Omega}{b_r\omega_\theta}\lambda \\ M_{\theta h} & 0 & M_{hh}\left(1-\lambda^2\frac{\omega_h^2}{\omega_\theta^2}\right) & M_{h\alpha} \\ M_{\theta\alpha} & -iM_{\psi\alpha}\frac{R\Omega}{b_r\omega_\theta}\lambda & M_{h\alpha} & M_{\alpha\alpha}\left(1-\lambda^2\frac{\omega_\alpha^2}{\omega_\theta^2}\right) \end{vmatrix} = 0 \qquad (C1)$$

where M_{ij} is defined by equation (B27). Values of $\lambda = \frac{\omega_\theta}{\omega}$ are desired for values of Ω/ω_θ. Expansion of the determinant gives a polynomial in λ^2 and $\left(\frac{\Omega}{\omega_\theta}\right)^2$ which can be written as:

$$\left(\frac{\Omega}{\omega_\theta}\right)^2 = \left(\frac{b_r}{R}\right)^2 \frac{M_{\psi\psi}\left(1-\frac{\omega_\psi^2}{\omega_\theta^2}\lambda^2\right)}{\lambda^2}\left(\frac{A_1\lambda^6 + A_2\lambda^4 + A_3\lambda^2 + A_4}{B_1\lambda^4 + B_2\lambda^2 + B_3}\right) \qquad (C2)$$

where

$$A_1 = -M_{hh}M_{\alpha\alpha}\left(\frac{\omega_\alpha}{\omega_\theta}\right)^2\left(\frac{\omega_h}{\omega_\theta}\right)^2$$

$$A_2 = M_{hh}M_{\alpha\alpha}\left[\left(\frac{\omega_\alpha}{\omega_\theta}\right)^2\left(\frac{\omega_h}{\omega_\theta}\right)^2 + \left(\frac{\omega_\alpha}{\omega_\theta}\right)^2 + \left(\frac{\omega_h}{\omega_\theta}\right)^2\right]$$

$$A_3 = -M_{hh}M_{\alpha\alpha}\left[1 + \left(\frac{\omega_\alpha}{\omega_\theta}\right)^2 + \left(\frac{\omega_h}{\omega_\theta}\right)^2\right] + M_{h\alpha}^2 + M_{\theta h}^2M_{\alpha\alpha}\left(\frac{\omega_\alpha}{\omega_\theta}\right)^2 + M_{\theta\alpha}^2M_{hh}\left(\frac{\omega_h}{\omega_\theta}\right)^2$$

$$A_4 = M_{hh}M_{\alpha\alpha} - M_{h\alpha}^2 + 2M_{\theta h}M_{\theta\alpha}M_{h\alpha} - M_{\theta h}^2M_{\alpha\alpha} - M_{\theta\alpha}^2M_{hh}$$

and

$$B_1 = M_{\theta\psi}^2M_{hh}M_{\alpha\alpha}\left(\frac{\omega_\alpha}{\omega_\theta}\right)^2\left(\frac{\omega_h}{\omega_\theta}\right)^2 + M_{\psi\alpha}^2M_{hh}\left(\frac{\omega_h}{\omega_\theta}\right)^2$$

$$B_2 = -M_{\theta\psi}^2M_{hh}M_{\alpha\alpha}\left[\left(\frac{\omega_\alpha}{\omega_\theta}\right)^2 + \left(\frac{\omega_h}{\omega_\theta}\right)^2\right] + 2M_{\theta\psi}M_{\theta\alpha}M_{\psi\alpha}M_{hh}\left(\frac{\omega_h}{\omega_\theta}\right)^2 - M_{\psi\alpha}^2M_{hh}\left[1 + \left(\frac{\omega_h}{\omega_\theta}\right)^2\right]$$

$$B_3 = M_{\theta\psi}^2M_{hh}M_{\alpha\alpha} - M_{\theta\psi}^2M_{h\alpha}^2 + 2M_{\theta\psi}M_{\theta h}M_{\psi\alpha}M_{h\alpha} - 2M_{\theta\psi}M_{\theta\alpha}M_{\psi\alpha}M_{hh} + M_{\psi\alpha}^2M_{hh} - M_{\theta h}^2M_{\psi\alpha}^2$$

Discussion and Application

Some observations can be made about the behavior of the mechanical system from inspection of equation (C2). For any value of λ, only one positive value of Ω/ω_θ is given by equation (C2); thus, the frequency of any one vibration mode cannot be the same as the frequency of any other mode at any value of Ω/ω_θ. Hence, if the frequencies of two vibration modes approach each other as Ω/ω_θ varies, the two curves of the frequency plot split and do not cross. Such frequency splits are also encountered in other vibrating systems (for example, see ref. 17). The numerator of equation (C2) gives the values of the coupled frequencies at Ω/ω_θ of zero. (Note that the yawing mode is uncoupled for Ω/ω_θ of zero.) The denominator of equation (C2) gives three asymptotes: $\lambda^2 = 0$, and the two roots of $B_1\lambda^4 + B_2\lambda^2 + B_3 = 0$. Thus, with the zeros, poles, and uniqueness of Ω/ω_θ for a given value of λ, the frequencies of the modes can be readily traced for variations of Ω/ω_θ.

Five cases are considered for illustration: two cases for configuration A, and one each for configurations B, C, and D. The results are presented in figure 15 for four modes and for only two modes, θ and ψ. These five cases vary widely in the location of the uncoupled engine frequencies relative to the wing frequencies. Figure 15 shows that the effects of increasing Ω/ω_θ may result in some cases in considerable differences in the values of the coupled frequencies from those at Ω/ω_θ of zero, depending upon the parameters of the system. A similar analysis showing the effect of gyroscopic coupling involving wing motion for one example is given in reference 18.

REFERENCES

1. Reed, Wilmer H., III, and Bland, Samuel R.: An Analytical Treatment of Aircraft Propeller Precession Instability. NASA TN D-659, 1961.

2. Sewall, John L.: An Analytical Trend Study of Propeller Whirl Instability. NASA TN D-996, 1962.

3. Ravera, Robert J.: Effects of Steady State Blade Angle of Attack on Propeller Whirl Flutter. Rep. No. ADR 06-01-63.1, Grumman Aircraft Eng. Corp., July 1963.

4. Reed, Wilmer H., III, and Bennett, Robert M.: Propeller Whirl Flutter Considerations for V/STOL Aircraft. Cal/Trecom Symposium Proceedings Vol II - Dynamic Load Problems Associated With Helicopters and V/STOL Aircraft, June 1963.

5. Houbolt, John C., and Reed, Wilmer H., III: Propeller-Nacelle Whirl Flutter. Jour. Aerospace Sci., vol. 29, no. 3, Mar. 1962, pp. 333-346.

6. Head, A. L., Jr.: A Review of the Structural Dynamic Characteristics of the XC-142A Aircraft. Cal/Trecom Symposium Proceedings Vol II - Dynamic Load Problems Associated With Helicopters and V/STOL Aircraft, June 1963.

7. Taylor, E. S., and Browne, K. A.: Vibration Isolation of Aircraft Power Plants. Jour. Aero. Sci., vol. 6, no. 2, Dec. 1938, pp. 43-49.

8. Bland, Samuel R., and Bennett, Robert M.: Wind-Tunnel Measurement of Propeller Whirl-Flutter Speeds and Static-Stability Derivatives and Comparison With Theory. NASA TN D-1807, 1963.

9. Abbott, Frank T., Jr., Kelly, H. Neale, and Hampton, Kenneth D.: Investigation of Propeller—Power-Plant Autoprecession Boundaries for a Dynamic-Aeroelastic Model of a Four-Engine Turboprop Transport Airplane. NASA TN D-1806, 1963.

10. Houbolt, John C., and Anderson, Roger A.: Calculations of Uncoupled Modes and Frequencies in Bending or Torsion of Nonuniform Beams. NACA TN 1522, 1948.

11. Yates, E. Carson, Jr.: Calculation of Flutter Characteristics for Finite-Span Swept or Unswept Wings at Subsonic and Supersonic Speeds by a Modified Strip Analysis. NACA RM L57L10, 1958.

12. Runyan, Harry L., and Watkins, Charles E.: Flutter of a Uniform Wing With an Arbitrarily Placed Mass According to a Differential-Equation Analysis and a Comparison With Experiment. NACA Rep. 966, 1950. (Supersedes NACA TN 1848.)

13. Woolston, Donald S., and Runyan, Harry L.: Appraisal of Method of Flutter Analysis Based on Chosen Modes by Comparison With Experiment for Cases of Large Mass Coupling. NACA TN 1902, 1949.

14. Yates, E. Carson, Jr.: Theoretical Investigation of the Subsonic and Supersonic Flutter Characteristics of a Swept Wing Employing a Tuned Sting-Mass Flutter Suppressor. NASA TN D-542, 1960.

15. Runyan, Harry L., and Sewall, John L.: Experimental Investigation of the Effects of Concentrated Weights on Flutter Characteristics of a Straight Cantilever Wing. NACA TN 1594, 1948.

16. Ribner, Herbert S.: Propellers in Yaw. NACA Rep. 820, 1945. (Supersedes NACA ARR 3L09.)

17. Silveira, Milton A., and Brooks, George W.: Analytical and Experimental Determination of the Coupled Natural Frequencies and Mode Shapes of a Dynamic Model of a Single-Rotor Helicopter. NASA MEMO 11-5-58L, 1958.

18. Scanlan, R. H., and Truman, John C.: The Gyroscopic Effect of a Rigid Rotating Propeller on Engine and Wing Vibration Modes. Jour. Aero. Sci., vol. 17, no. 10, Oct. 1950, pp. 653-659, 666.

TABLE I.- MASS PARAMETERS

(a) Propeller and power plant (pivoted)

Configuration	M_P, slugs	i_θ or i_ψ, slug-ft^2	I_Ω, slug-ft^2	s_θ, slug-ft
A	0.2388	0.0634	0.00858	0.03801
B	.1978	.04148	.00858	.009128
C	.1379	.01772	.00858	-.02849
D	.1379	.01709	.00858	-.02849

(b) Nacelle and mounting beam (nonpivoted mass)

Configuration	Mass, slugs	Inertia, slug-ft^2 (a)	Static unbalance, slug-ft (a)
A	0.1814	0.2237	-0.1496
B	.2224	.2783	-.1962
C	.2823	.3667	-.2689
D	.2823	.3674	-.2689

[a]Values given are relative to the elastic axis of the wing.

TABLE II.- MODEL TEST DATA

$\beta_{0.75R}$, deg	f_θ, cps	f_ψ, cps	$2\zeta_\theta$	$2\zeta_\psi$	ρ, slugs/cu ft	n, rps	V_f, ft/sec	f_f, cps
				Configuration A				
25	9.21	9.34	0.0072	0.0132	0.00230	61.5	125	5.70
35	↓	↓	↓	↓	↓	41.0	121	6.58
46						29.0	126	7.24
52						25.0	135	7.40
58						21.5	148	7.67
35	9.62	9.67	.0074	.0091		47.0	138	6.71
25	9.76	9.60	↓	↓		67.5	138	5.81
35	↓	↓				48.0	143	6.66
46			.0090	.0108		33.5	144	7.40
52			↓	↓		28.0	151	7.70
58						23.5	162	7.89
52	10.17	10.01	.0089	.0094		28.5	154	8.28
25	10.55	10.47	↓	↓		67.5	143	6.38
35	↓	↓				50.5	149	7.30
46						34.5	149	7.92
52						28.0	151	8.40
58				.0107		24.0	168	8.46
52	10.35	10.1	.0091	.0112		26.0	141	8.40
25	10.45	10.5	.0149	.0153		65.5	128	6.47
35	↓	↓	↓	↓		42.0	125	7.78
46						31.0	134	8.29
58						22.8	156	8.78
25	11.0	11.0	.0084	.0088		68.0	132	7.06
35	↓	↓	↓	↓		46.0	128	8.00
46						35.0	143	8.68
52						31.0	162	8.79
52	11.25	11.25	.0106	.0120	.00236	30.5	163	9.09
58	↓	↓	↓	↓	↓	26.0	177	9.20
35	11.6	11.7	.0290	.0324	.00231	63.5	188	7.60
46	↓	↓	↓	↓	.00230	46.5	202	8.41
52					.00228	40.0	216	8.60
58					.00233	36.0	251	8.94
				Configuration B				
25	14.4	14.6	0.0351	0.0299	0.00226	100	201	6.58
35	↓	↓	↓	↓	↓	68.0	201	7.97
40						60.5	218	8.46
46						53.0	232	8.80
52						49.0	274	8.96
				Configuration C				
25	19.4	20.0	0.0289	0.0266	0.00233	90.5	185	6.16
30	↓	↓	↓	↓	↓	72.0	177	7.11
35						62.0	181	7.96
46						52.0	229	8.44
52						50.0	281	8.26
				Configuration D				
25	7.95	23.5	0.0367	0.0310	0.00233	66.0	130	3.95
35	↓	↓	↓	↓	↓	48.5	138	4.69
46						37.0	155	5.09
52						32.5	171	5.09
58						29.0	199	4.86
58	7.64	23.3	.0292	.0199	↓	27.5	189	5.03

TABLE III.- PROPELLER AERODYNAMIC QUANTITIES USED IN THE ANALYSIS

$\beta_{0.75R}$, deg	J	e_θ or e_ψ	C_{m_θ}	C_{Z_θ}	C_{m_ψ}	C_{Z_ψ}	C_{m_q}
25	1.25	-0.31092	0.0447	-0.232	0.0985	0.0996	-0.1574
35	1.80	-.31781	.0382	-.295	.0964	.1018	-.1126
46	2.66	-.32446	.0296	-.364	.0866	.1028	-.0738
52	3.31	-.32758	.0253	-.402	.0801	.1032	-.0525
58	4.21	-.33031	.0213	-.440	.0734	.1040	-.0361

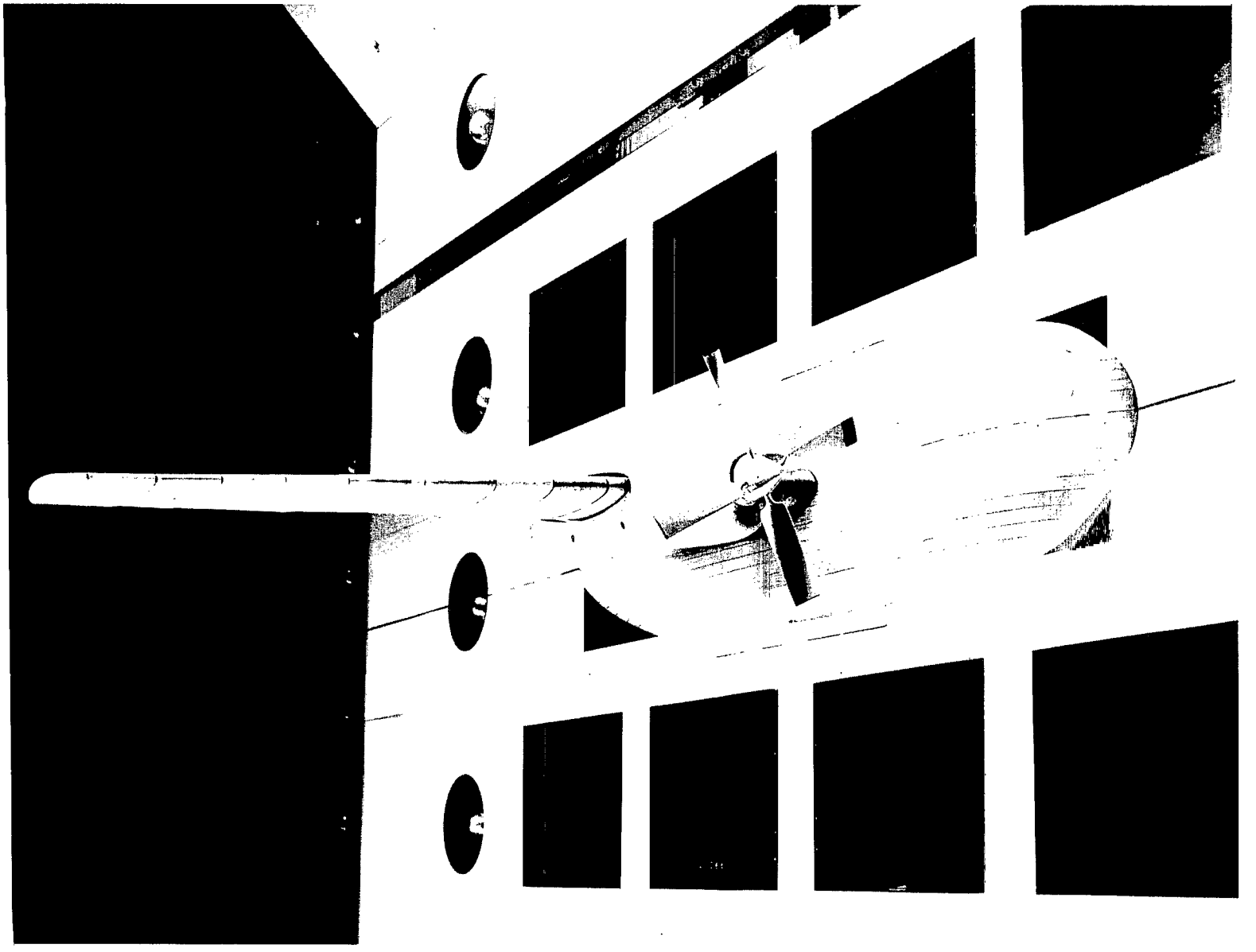

L-61-291

Figure 1.- Photograph of model in the test section of the Langley transonic dynamics tunnel.

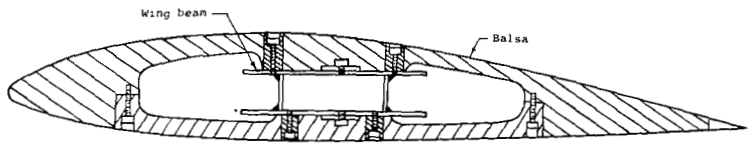

(a) Typical section through wing.

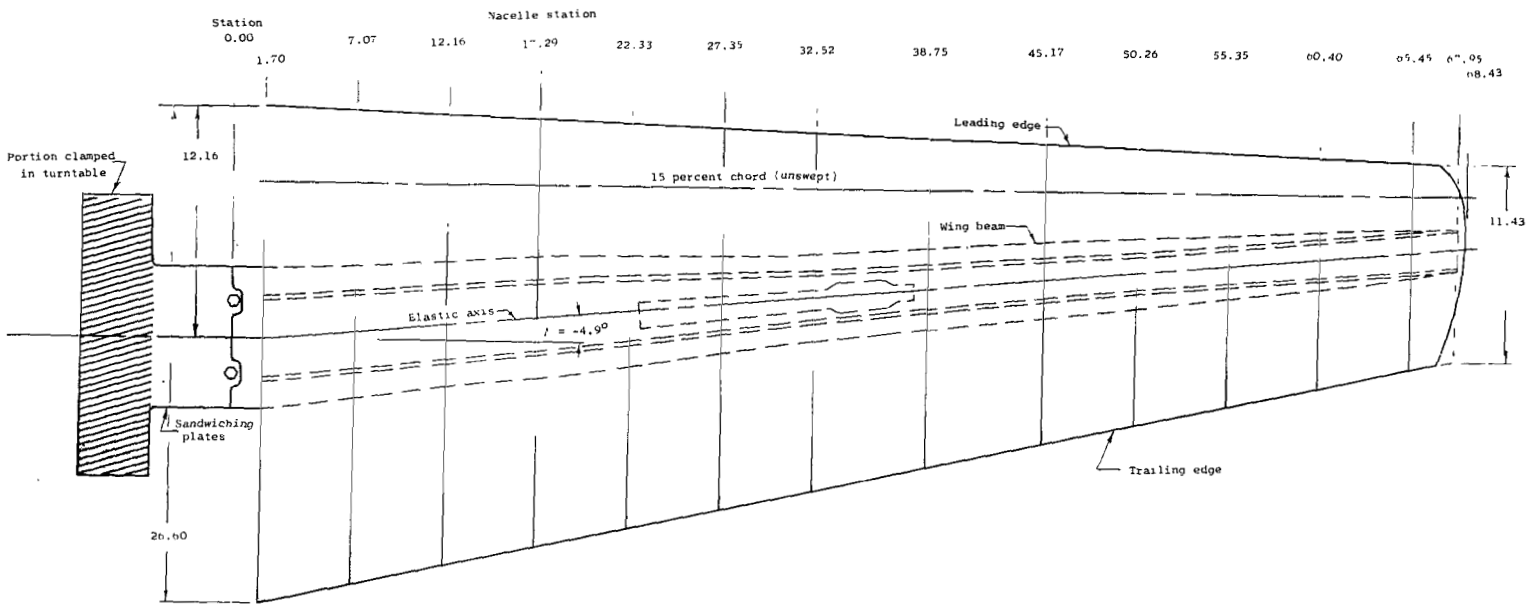

(b) Plan view.

Figure 2.- Schematic of wing showing layout of spar and balsa pods. All dimensions are given in inches.

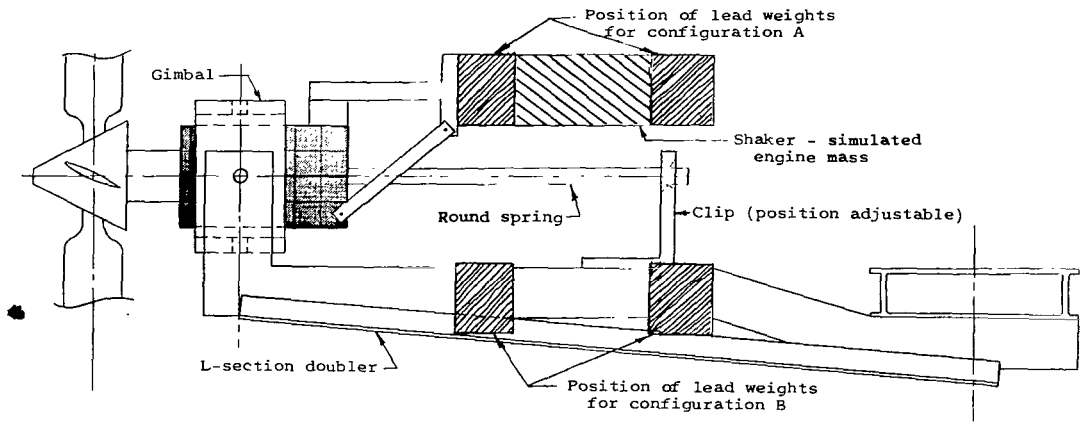

(a) Configurations A and B.

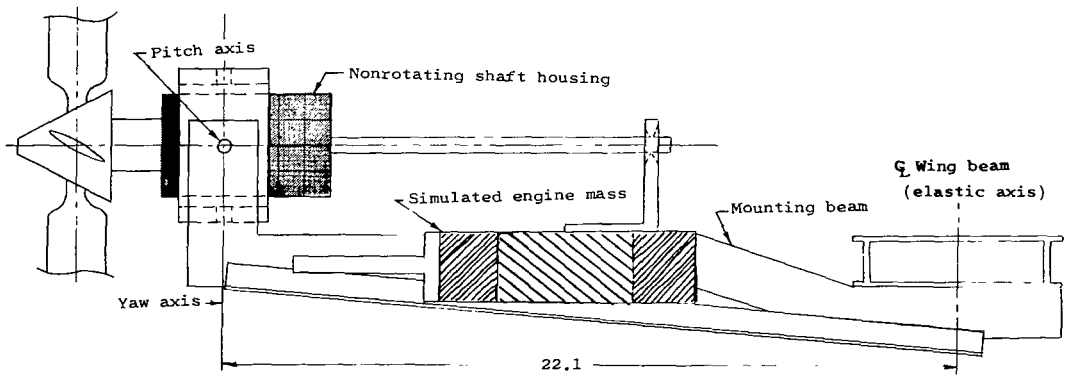

(b) Configuration C.

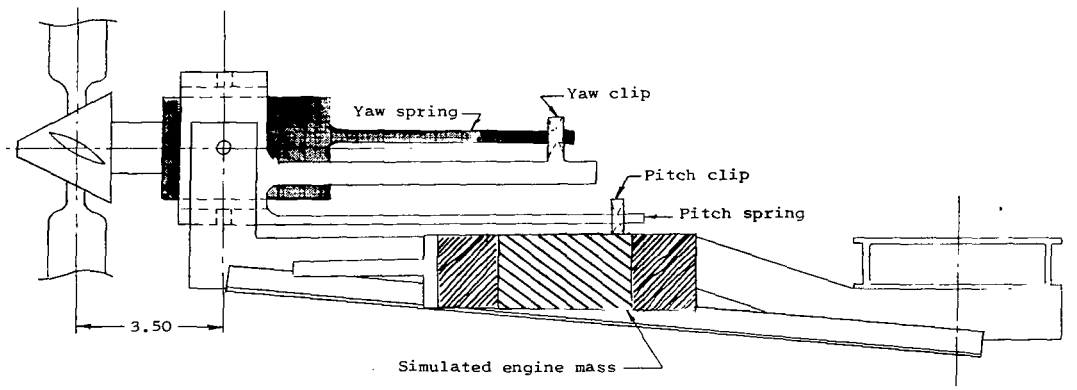

(c) Configuration D.

Figure 3.- Schematic representation of power-plant arrangement for each configuration. All dimensions in inches.

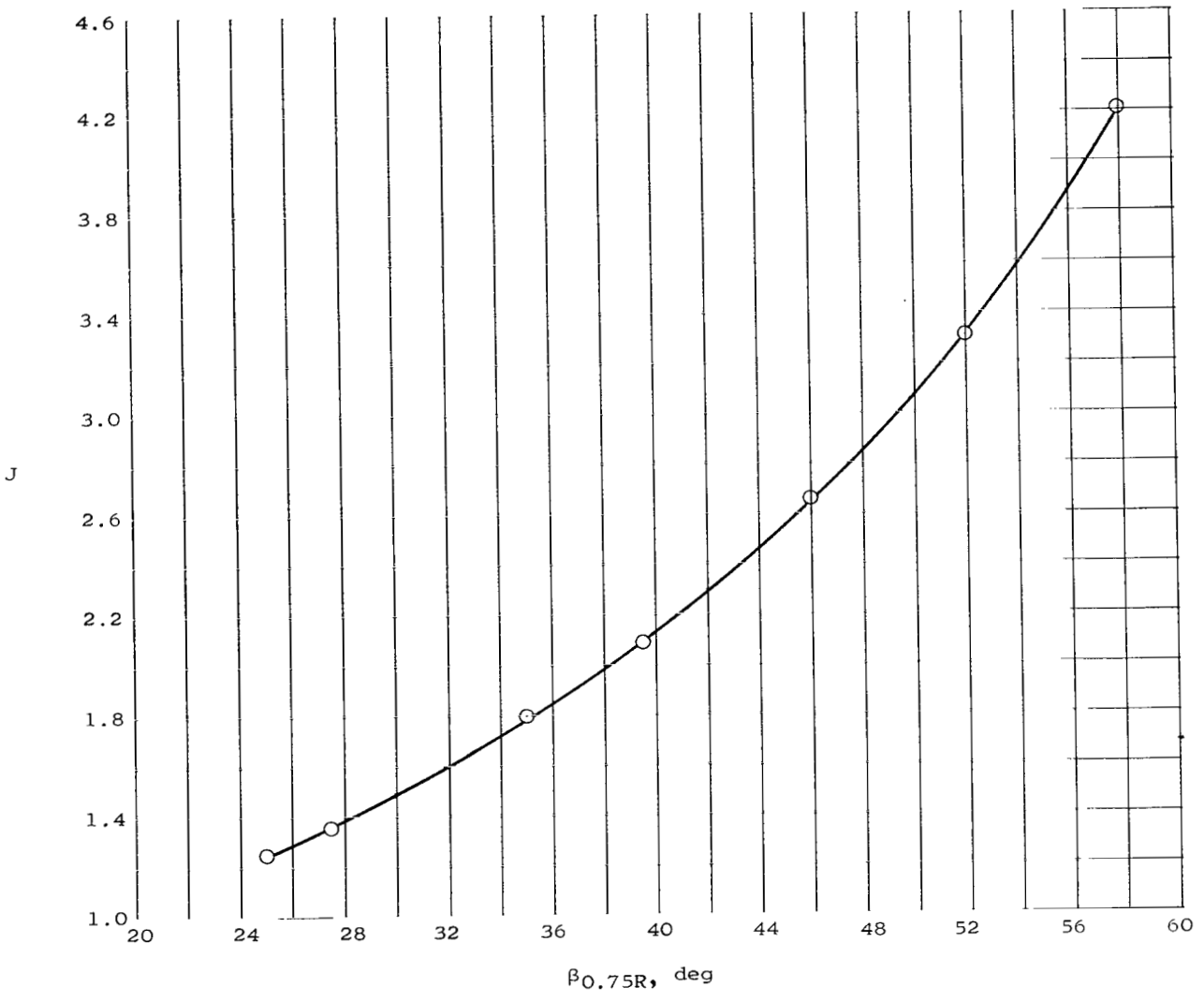

Figure 4.- Experimental variation of advance ratio with geometric blade angle at three-quarter blade radius for windmilling propeller (ref. 8).

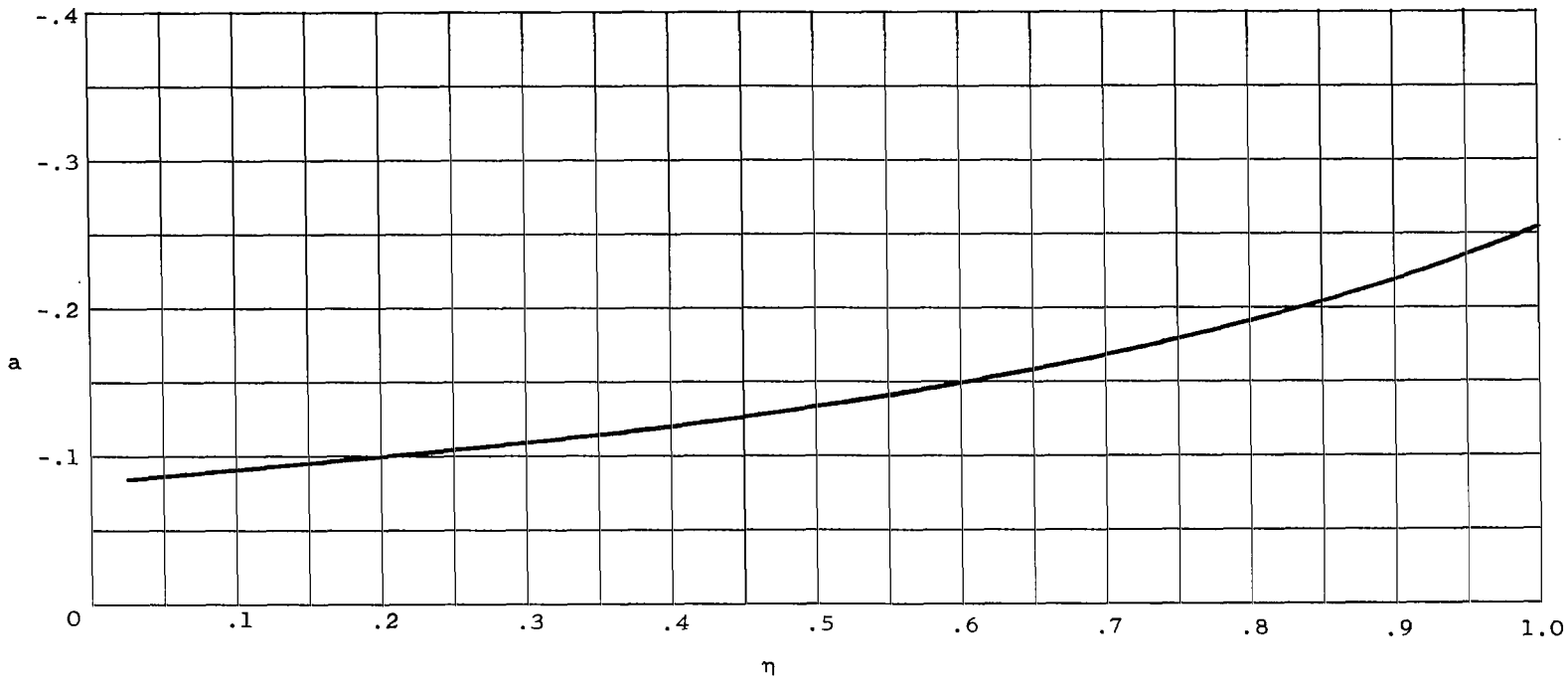

Figure 5.- Nondimensional position of elastic axis along the wing span.

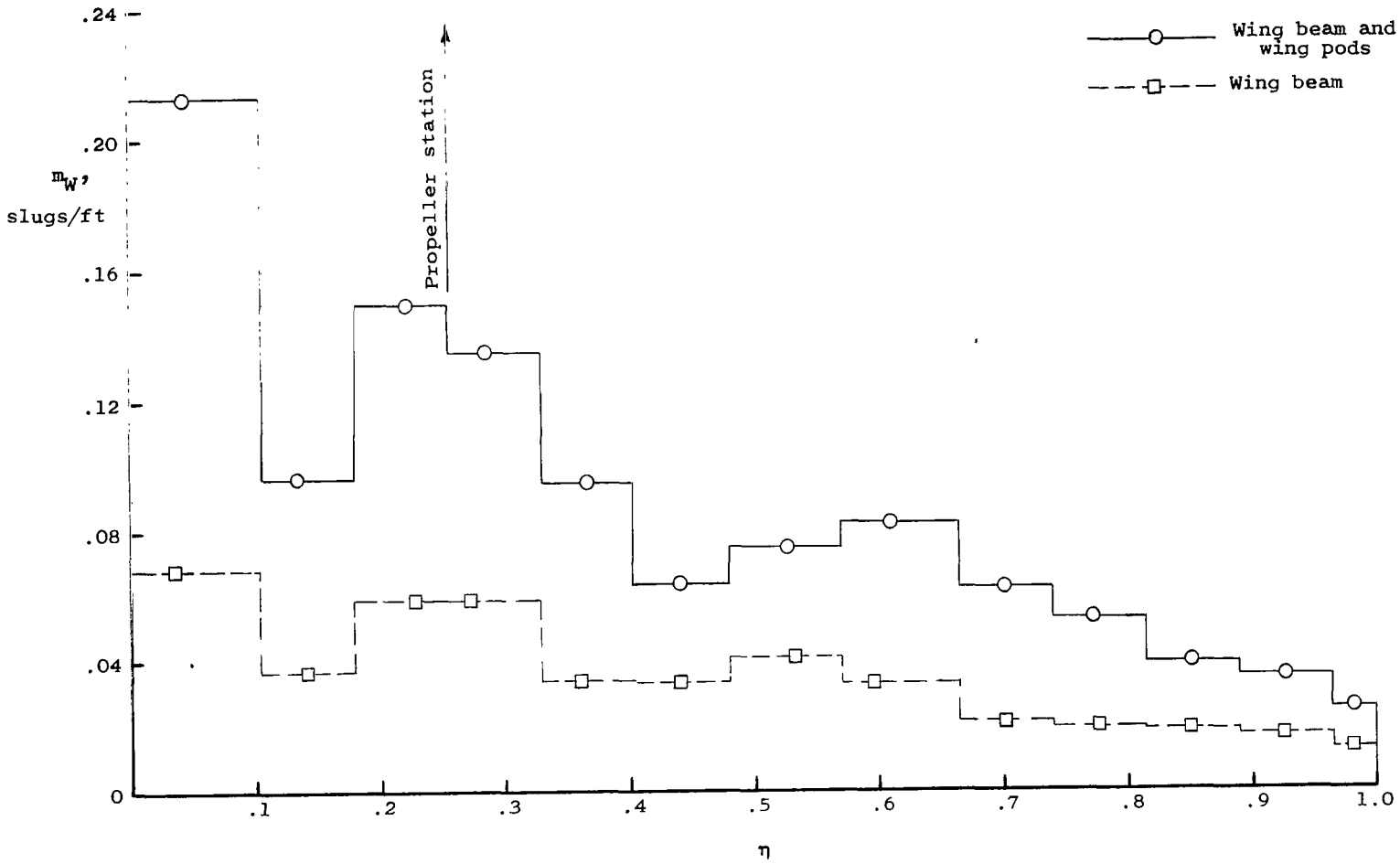

(a) Mass.

Figure 6.- Distribution of wing mass parameters along the wing span. Symbols indicate position along the span of the center of gravity of each strip. Parameters for nacelle and mounting beam are given in table I(b).

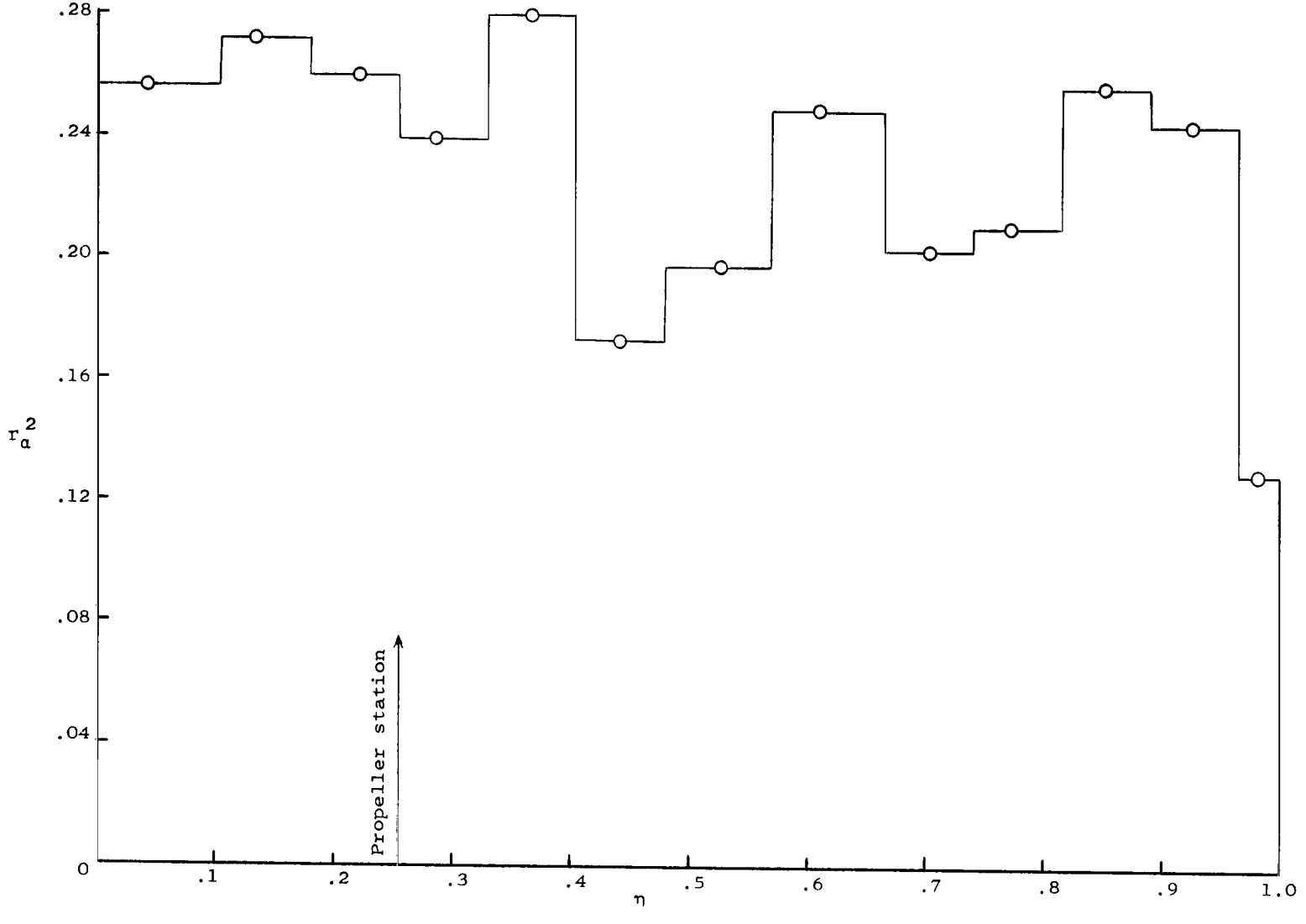

(b) Nondimensional inertia parameter.

Figure 6.- Continued.

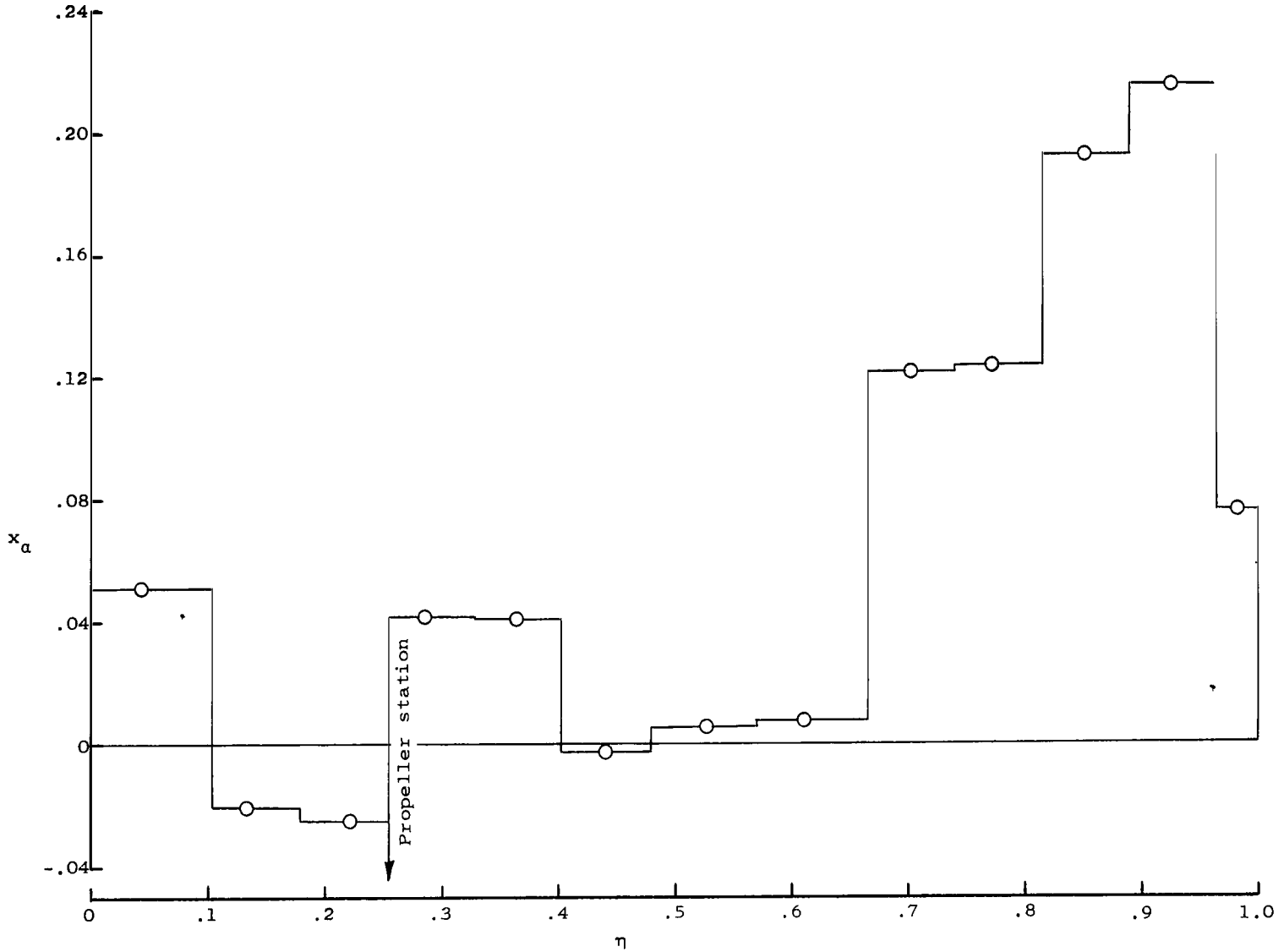

(c) Nondimensional static unbalance parameter.

Figure 6.- Concluded.

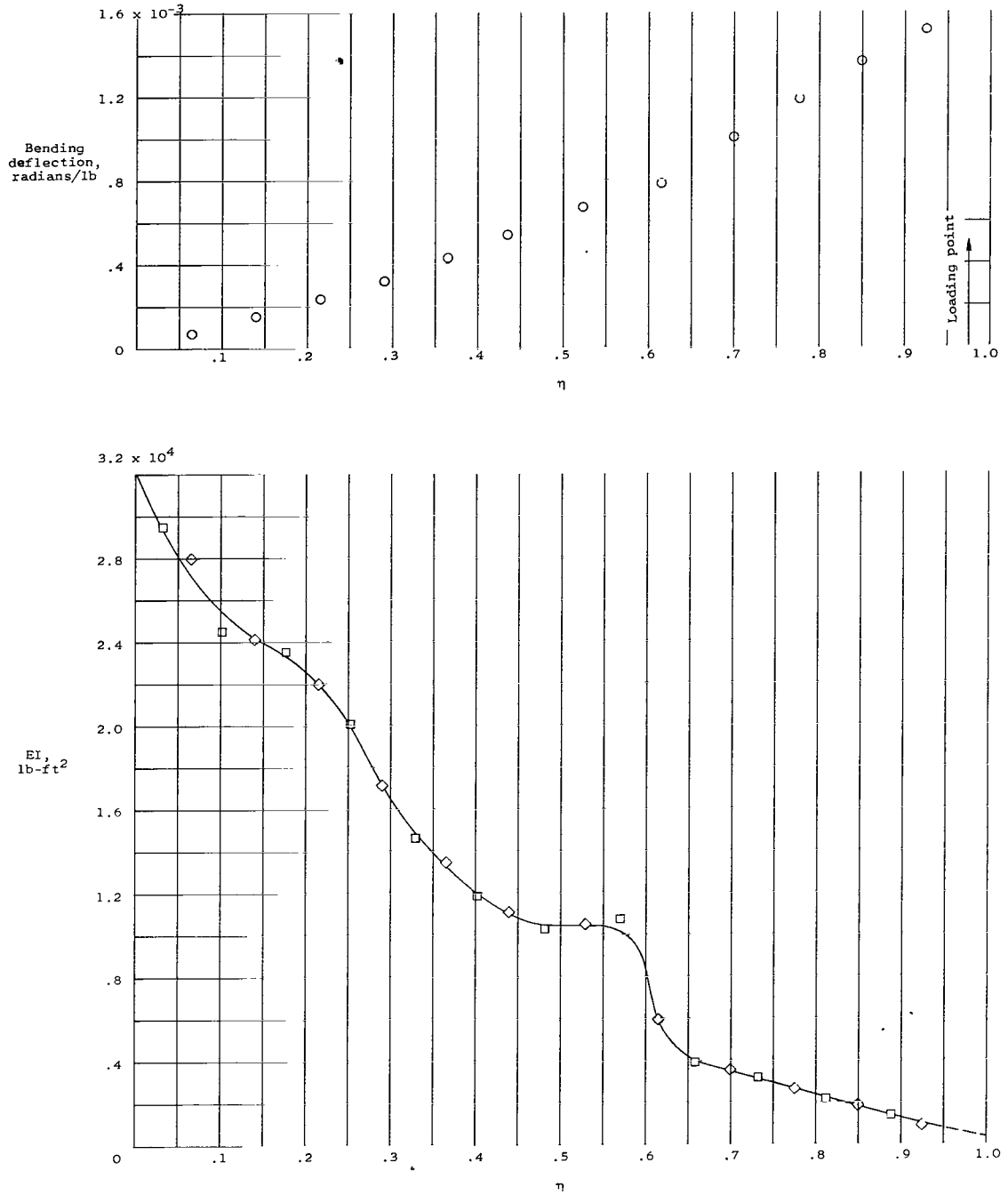

(a) Stiffness and slope of static deflection curve in bending.

Figure 7.- Spanwise distribution of stiffnesses and slopes of static deflection curves. Square symbols indicate values obtained by numerical differentiation of the slopes between data points; diamonds correspond to values obtained by numerical differentiation at data points.

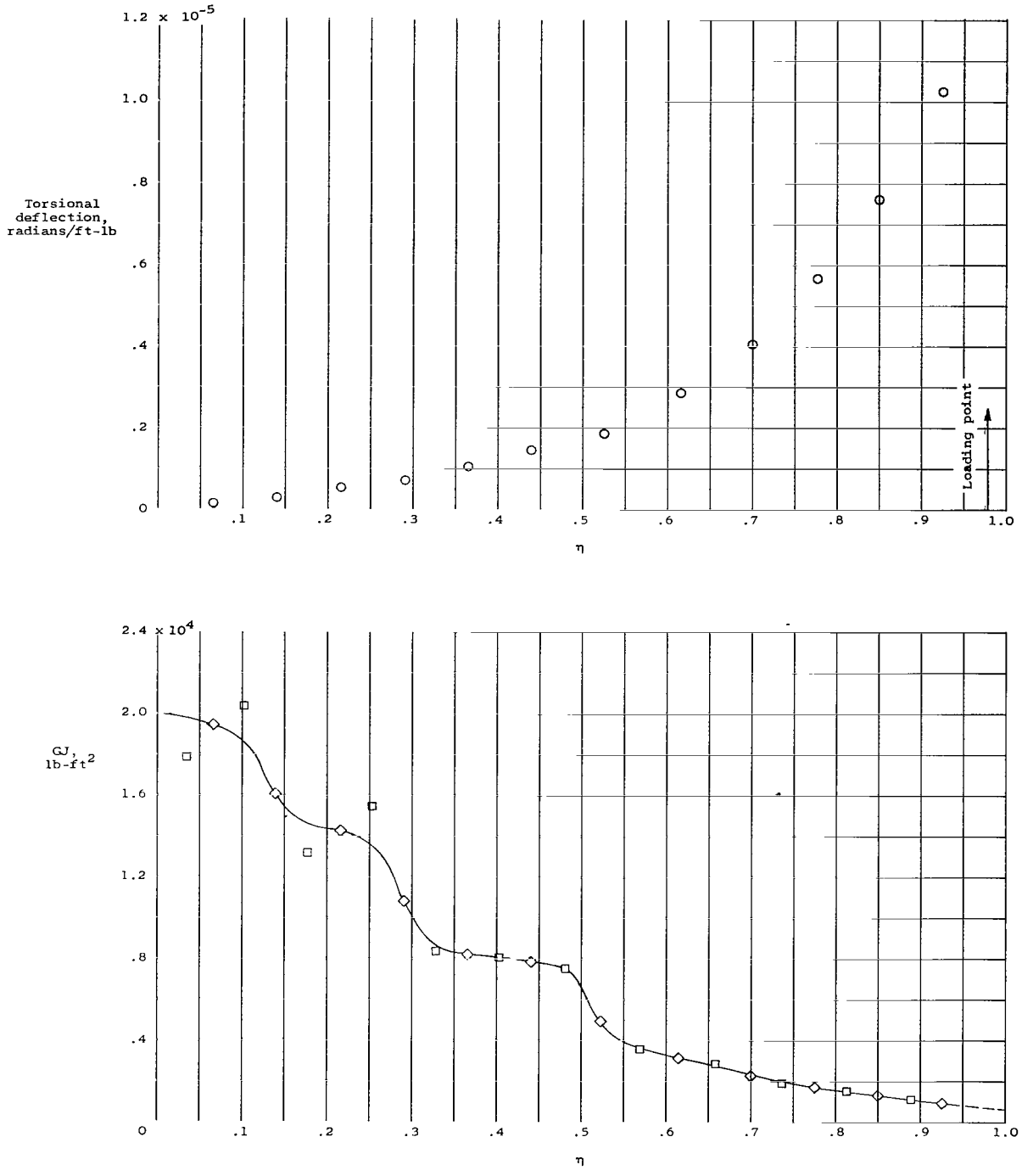

(b) Stiffness and slope of static deflection curve in torsion.

Figure 7.- Concluded.

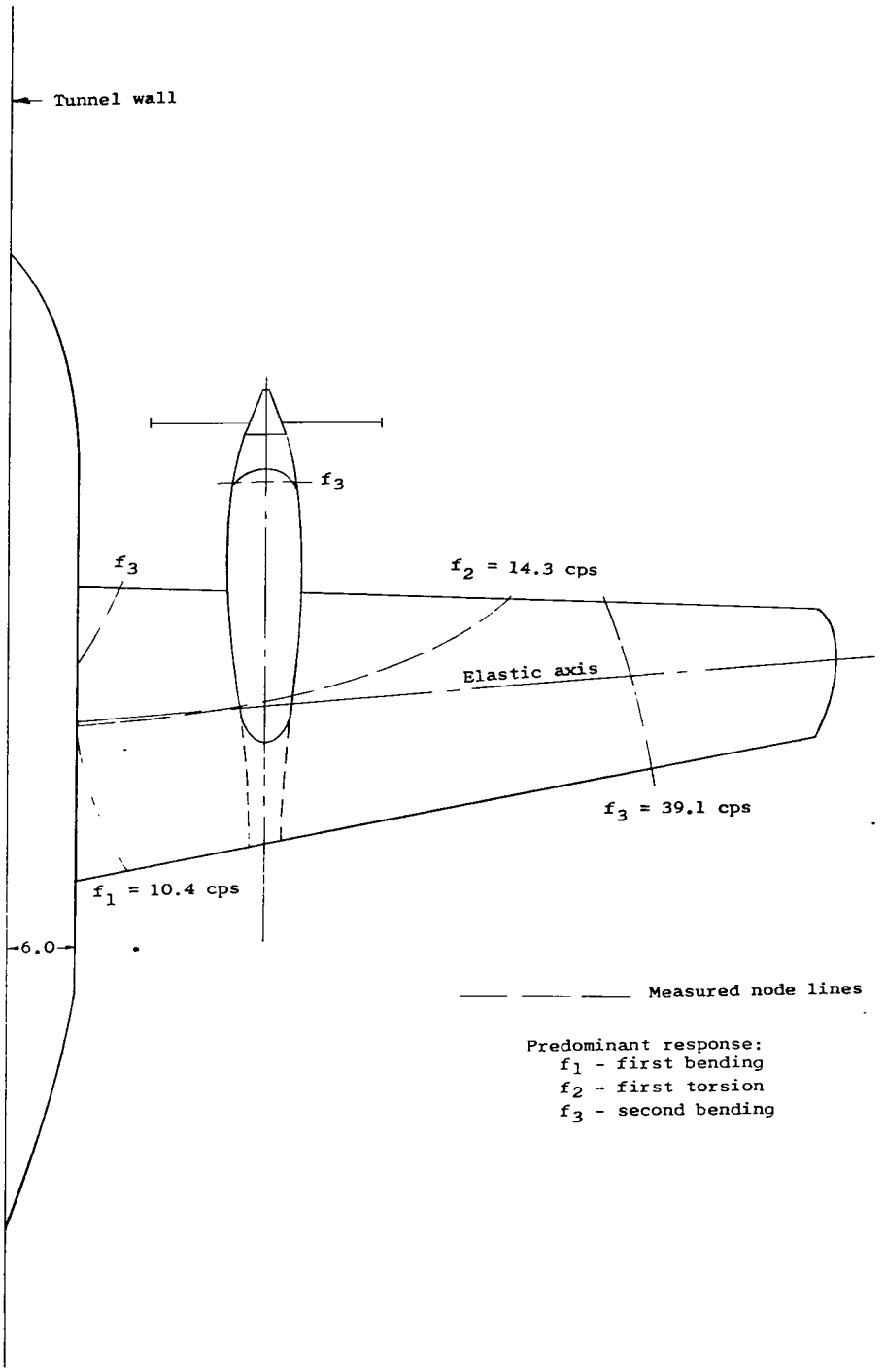

Figure 8.- Sketch of layout of model in tunnel showing measured node lines and frequencies of modes that involved primarily wing motion for configuration A, $f_\theta = f_\psi = 9.3$ cps. All dimensions in inches unless otherwise specified.

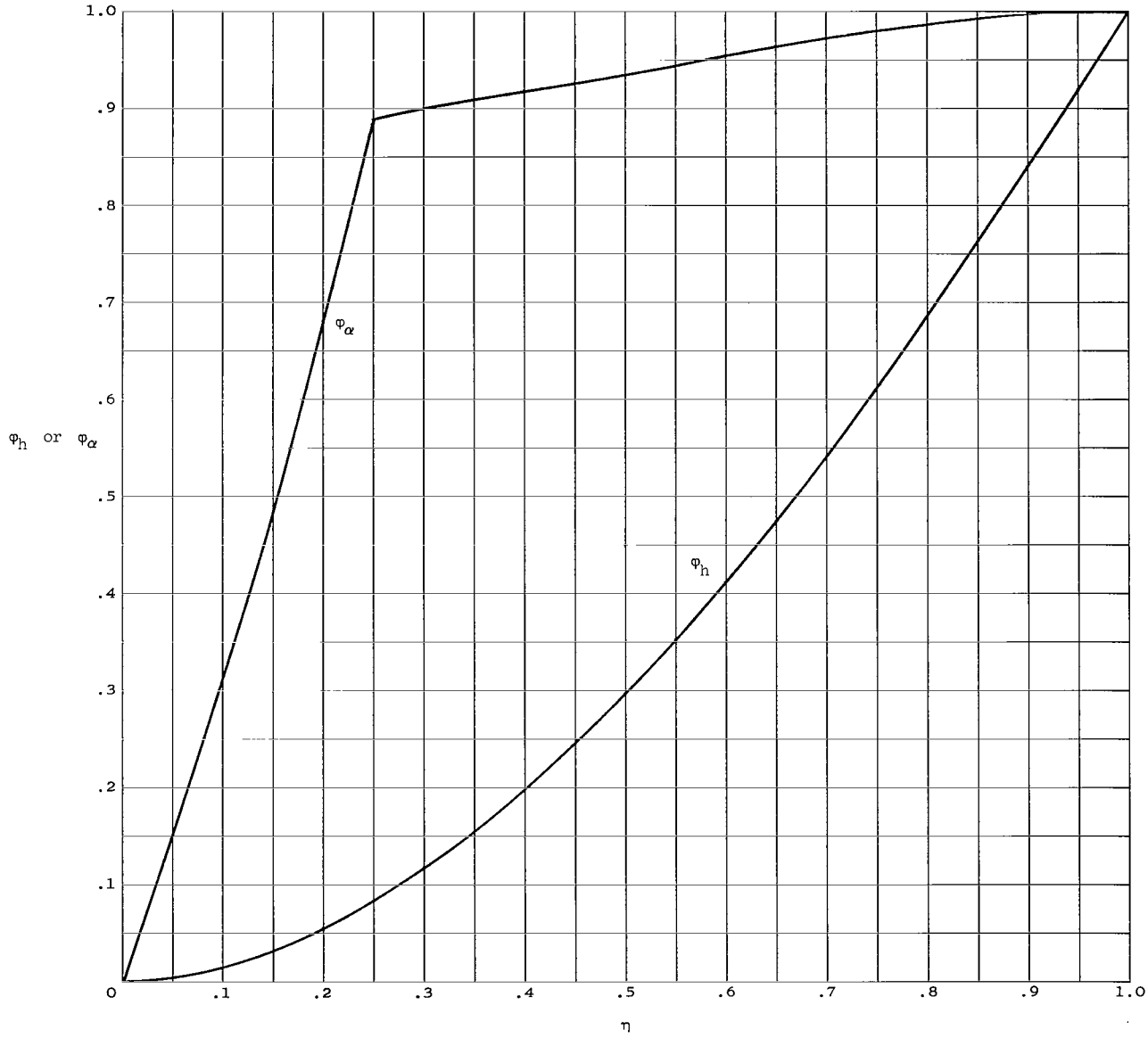

Figure 9.- Calculated uncoupled mode shapes of vibration for the model.

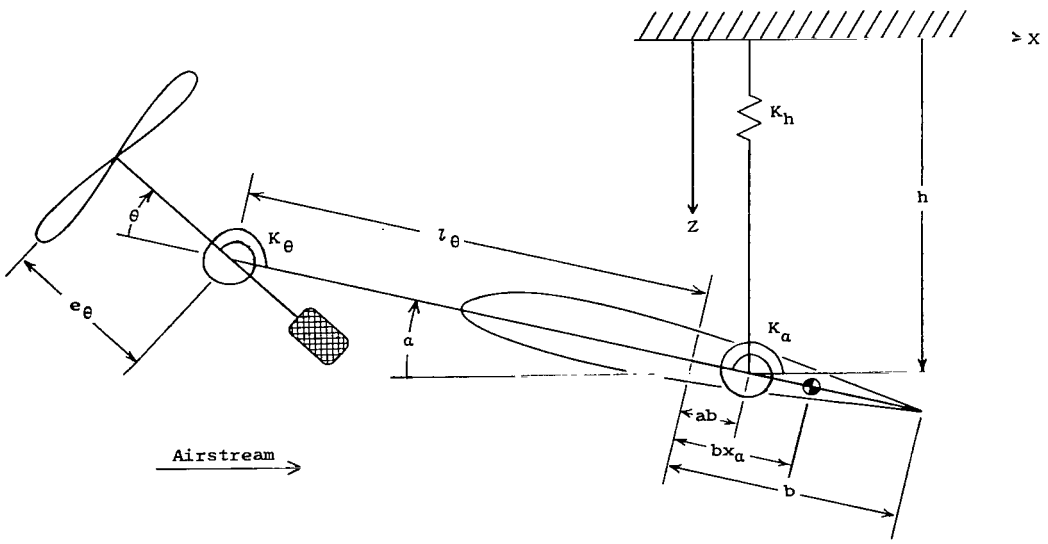

(a) Section at propeller station.

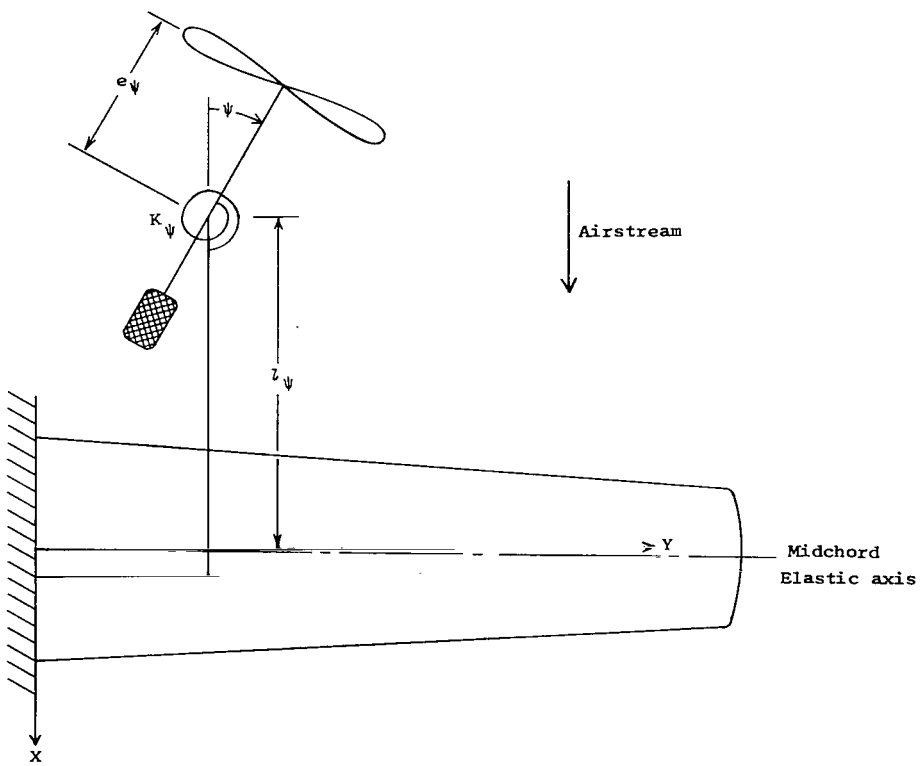

(b) Plan view.

Figure 10.- Sketch of model as treated in analysis.

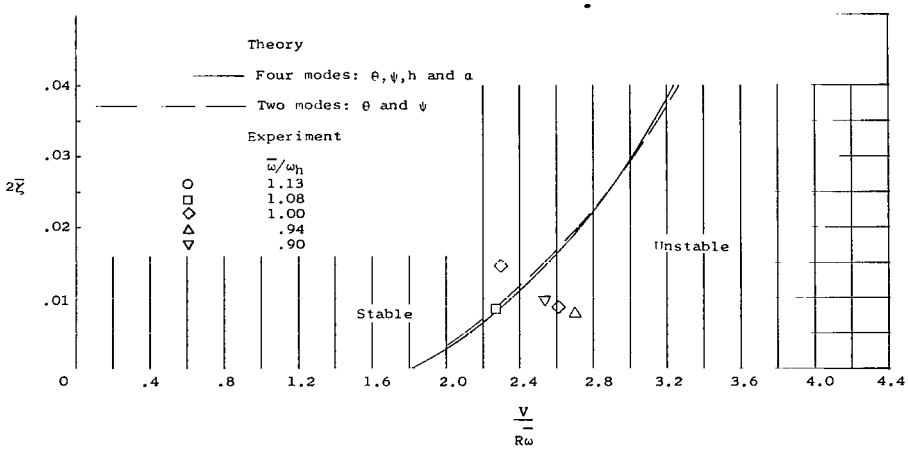

(a) $\beta_{0.75R} = 25^{\circ}$.

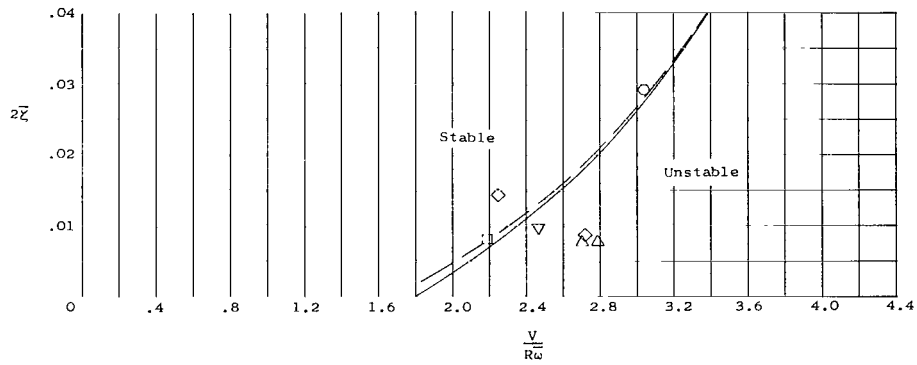

(b) $\beta_{0.75R} = 35^{\circ}$.

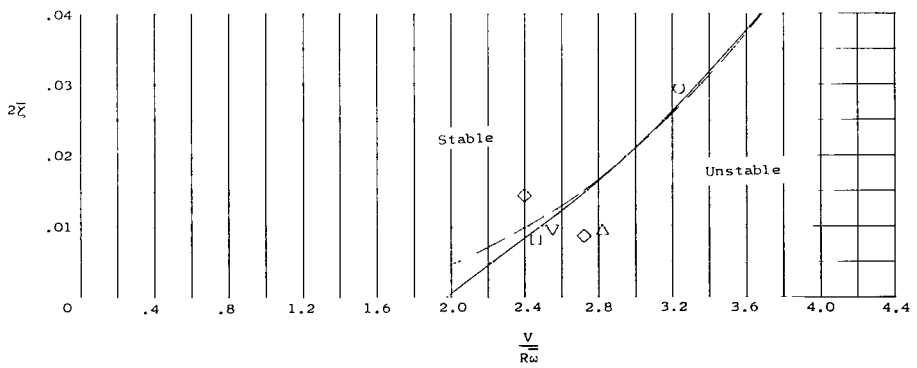

(c) $\beta_{0.75R} = 46^{\circ}$.

Figure 11.- Comparison of experimental and theoretical whirl flutter speeds for configuration A.

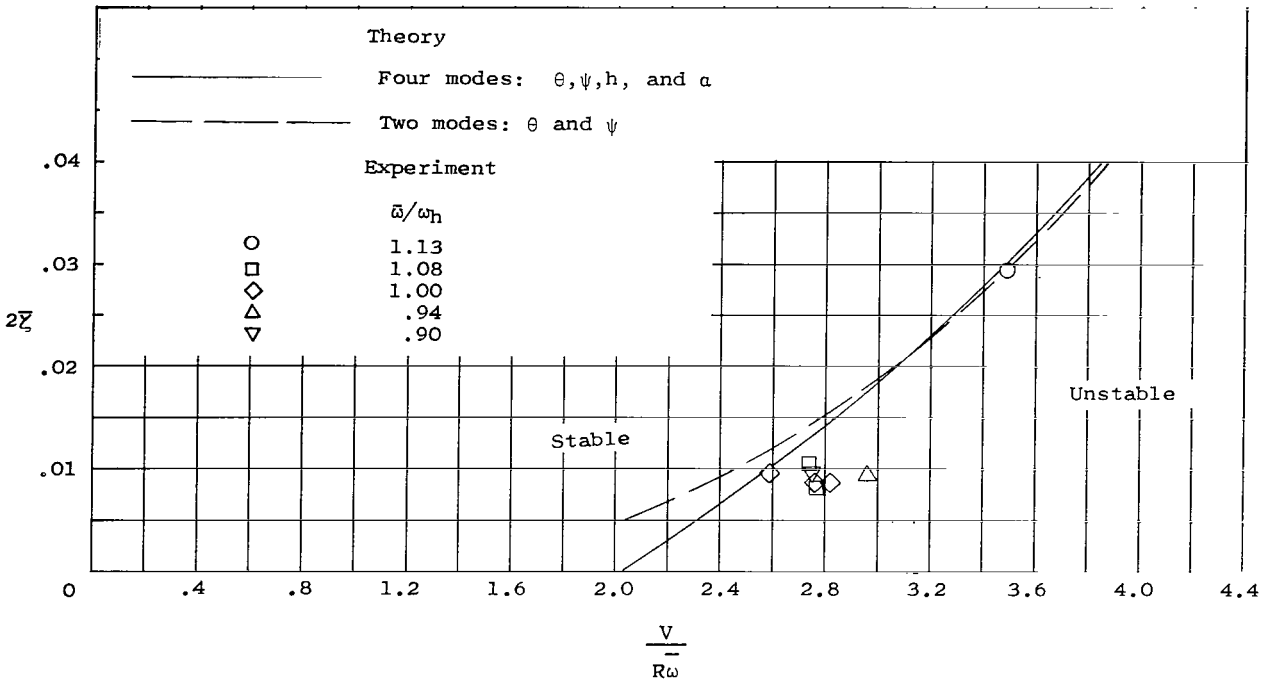

(d) $\beta_{0.75R} = 52^{\circ}$.

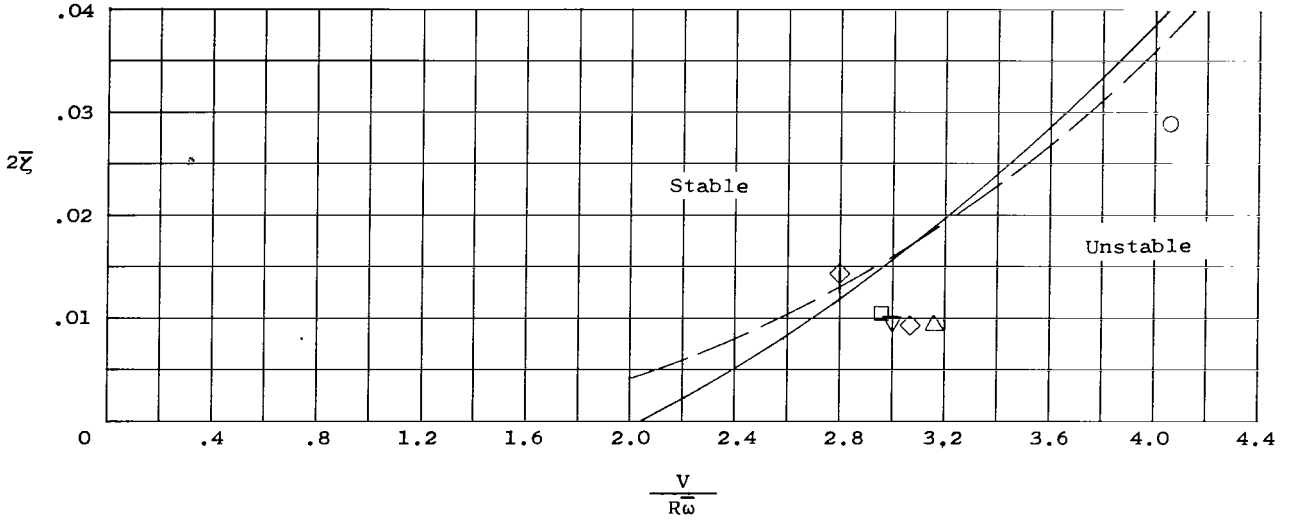

(e) $\beta_{0.75R} = 58^{\circ}$.

Figure 11.- Concluded.

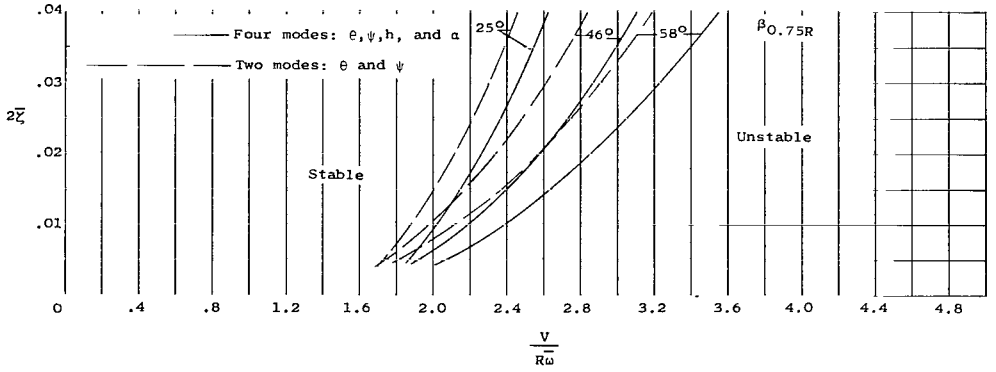

(a) Configuration B.

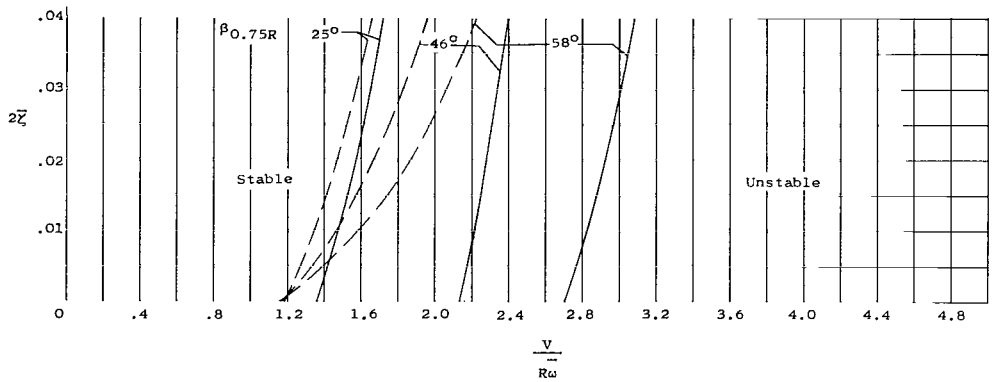

(b) Configuration C.

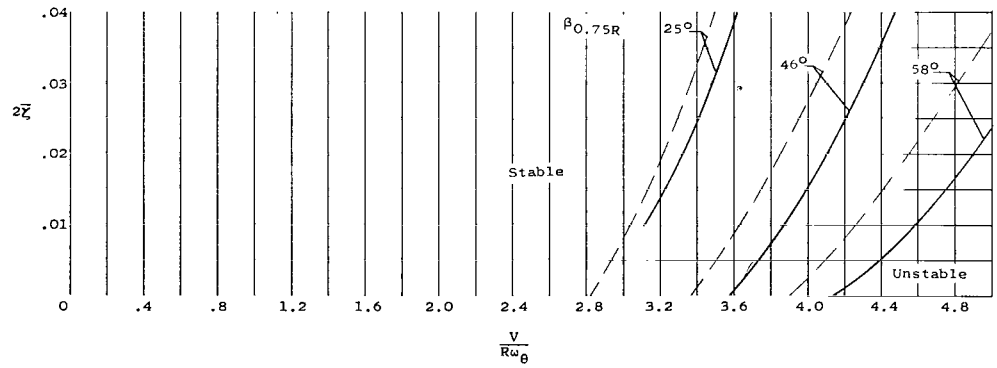

(c) Configuration D.

Figure 12.- Comparison of theoretical whirl flutter speeds with and without wing flexibility.

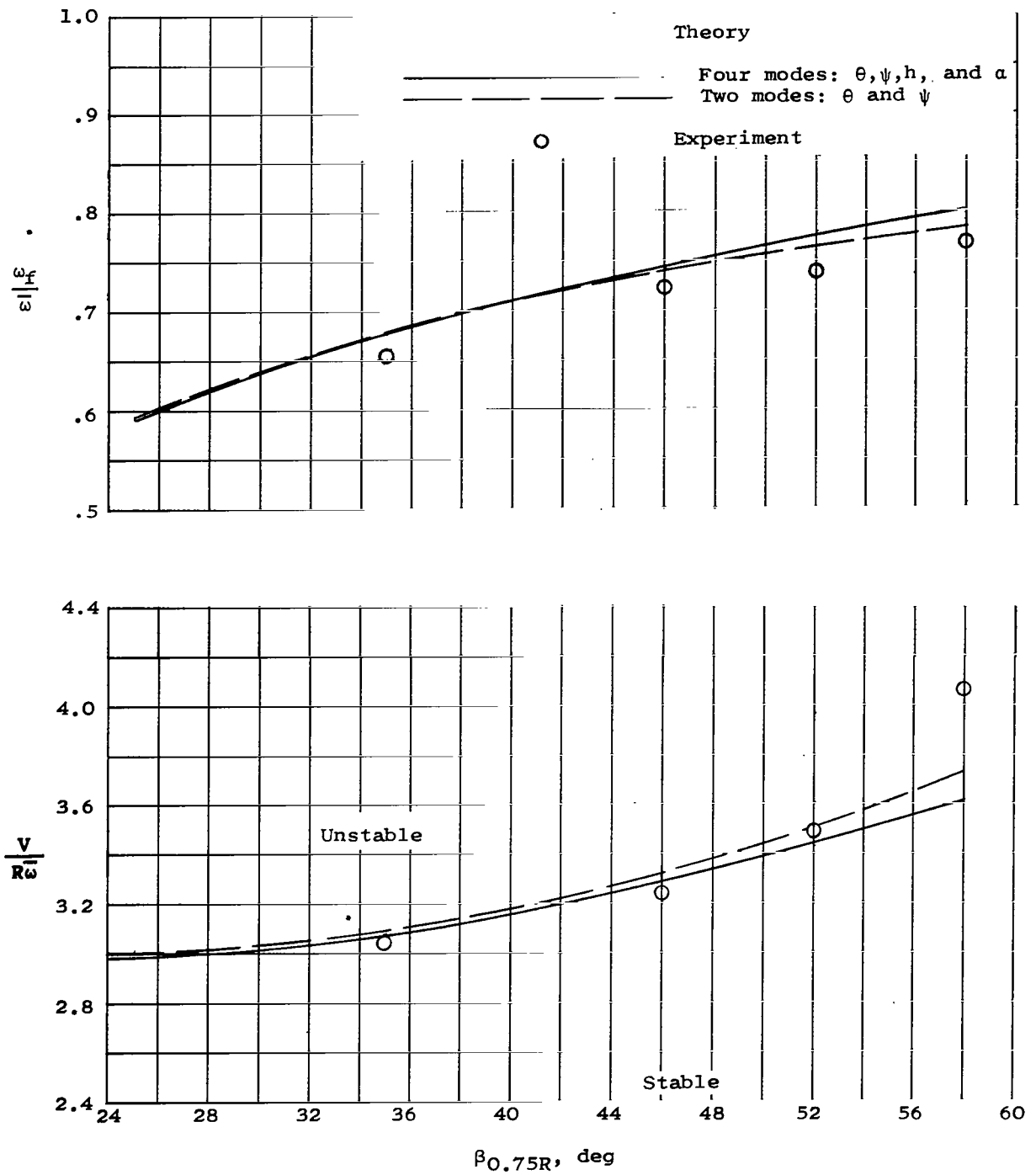

(a) Configuration A, $2\bar{\zeta} = 0.029$.

Figure 13.- Comparison of experimental and theoretical whirl flutter speeds and frequencies.

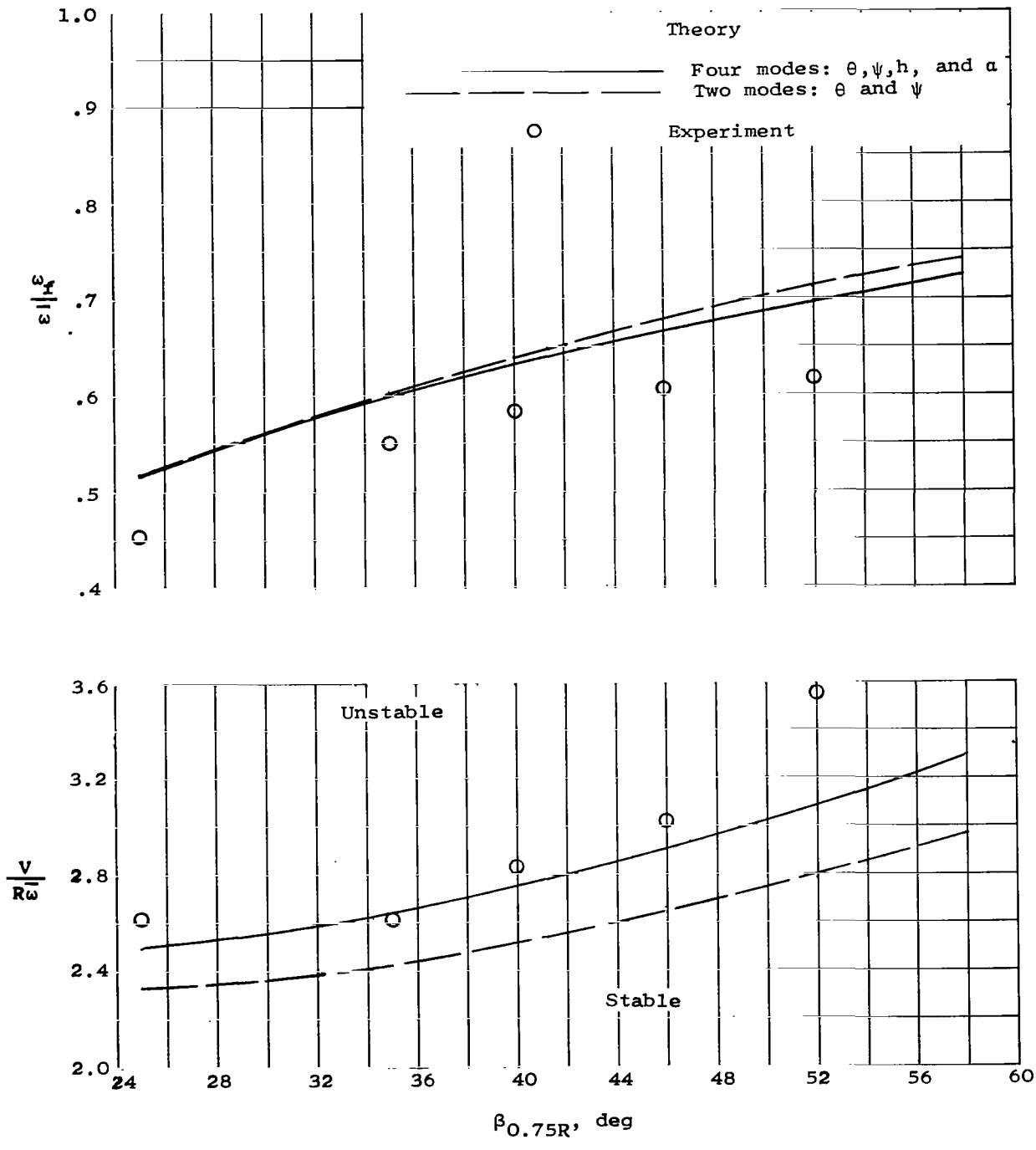

(b) Configuration B, $2\bar{\zeta} = 0.032$.

Figure 13.- Continued.

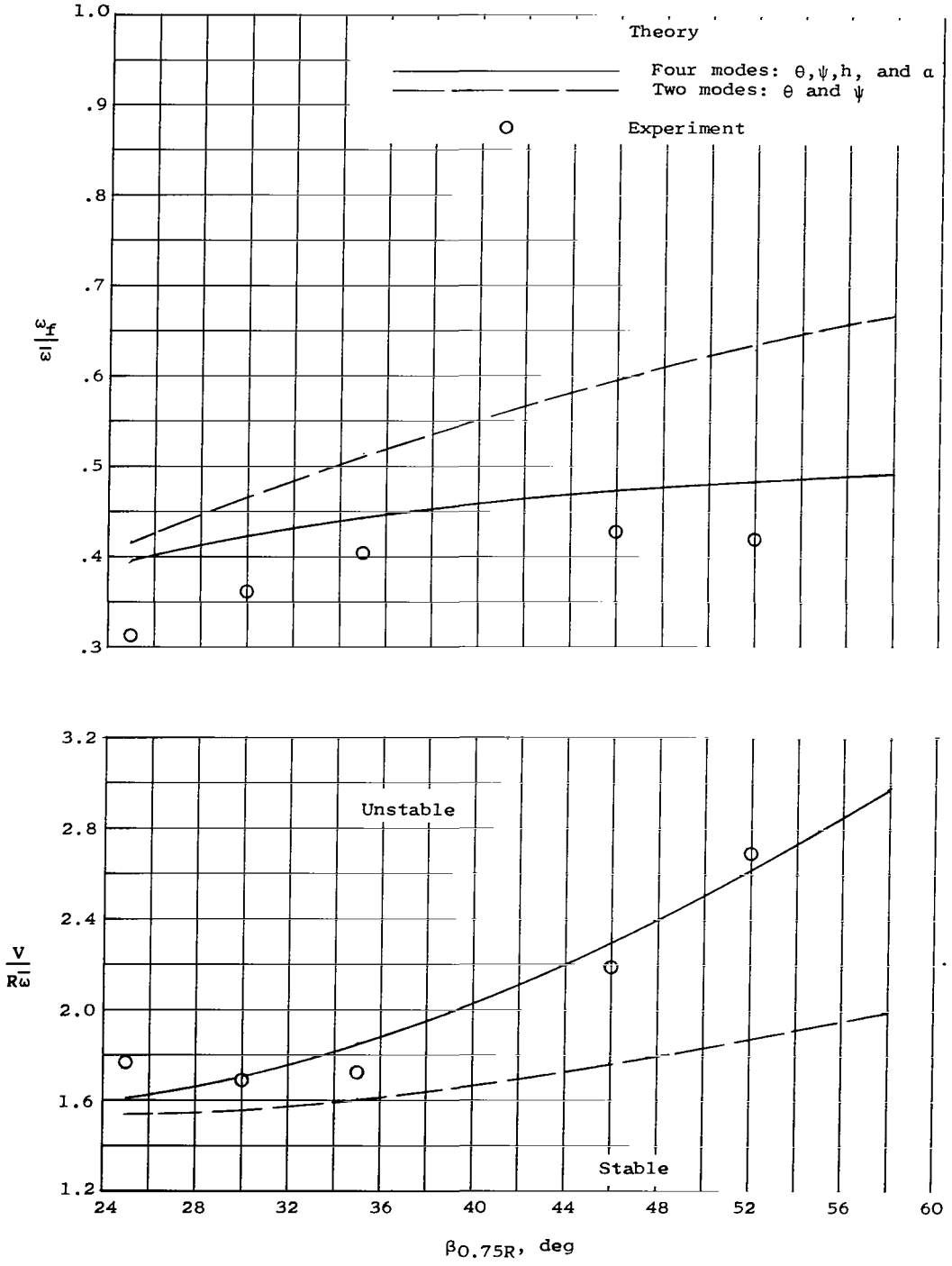

(c) Configuration C, $2\bar{\zeta} = 0.026$.

Figure 13.- Continued.

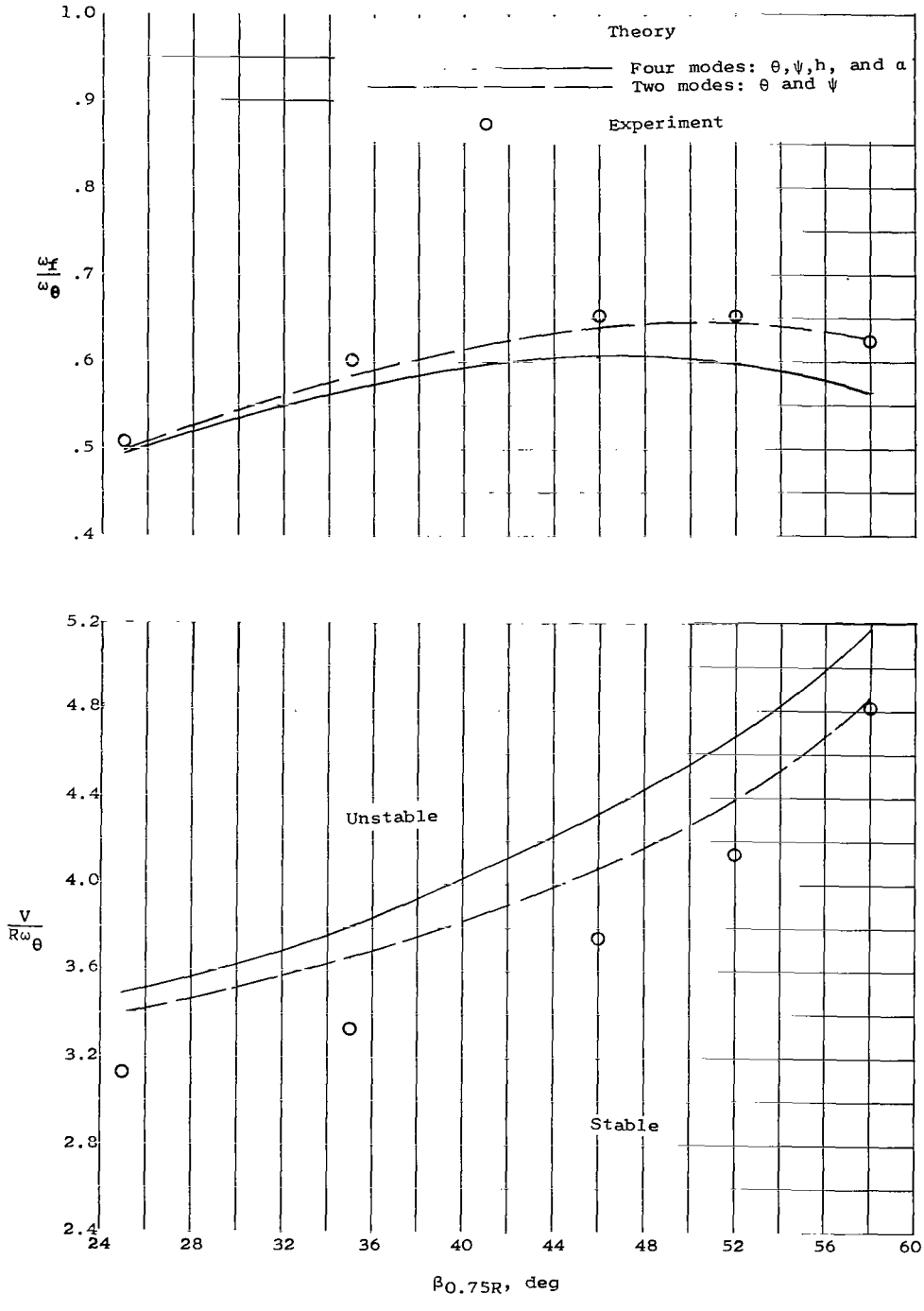

(d) Configuration D, $2\bar{\zeta} = 0.032$.

Figure 13.- Concluded.

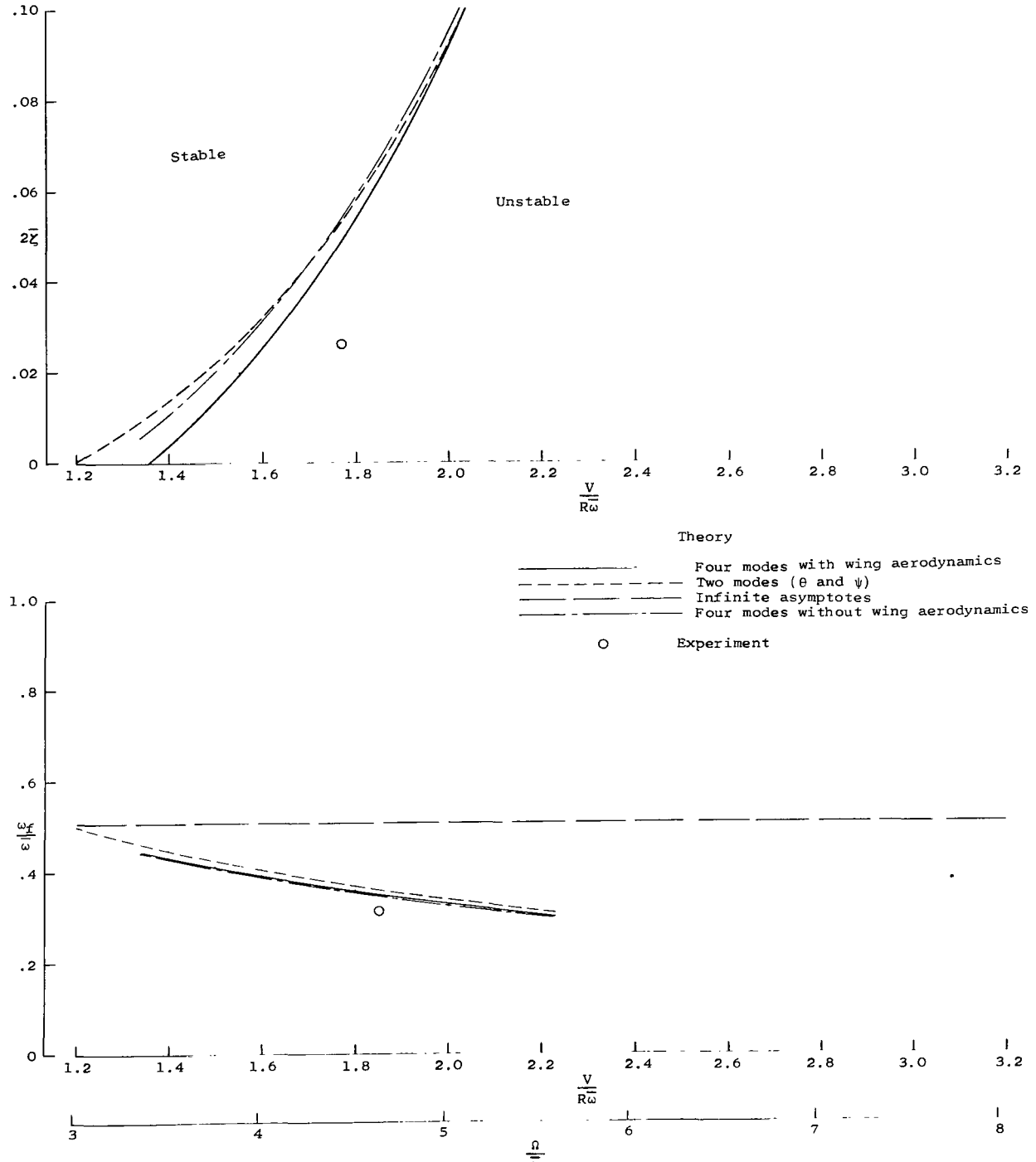

(a) $\beta_{0.75R} = 25^{\circ}$.

Figure 14.- Effect of wing aerodynamics on flutter characteristics for configuration C.

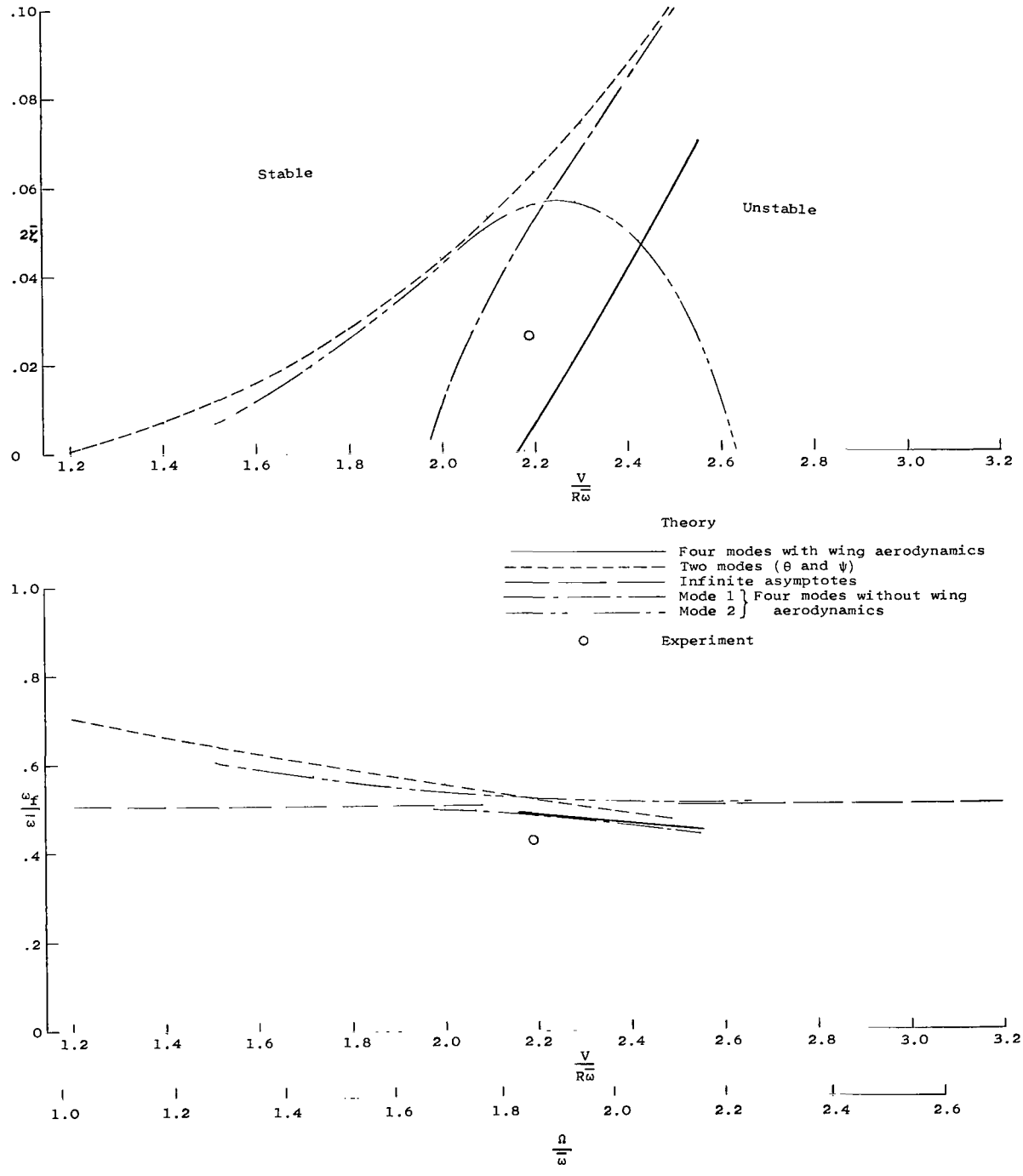

(b) $\beta_{0.75R} = 46^{\circ}$.

Figure 14.- Continued.

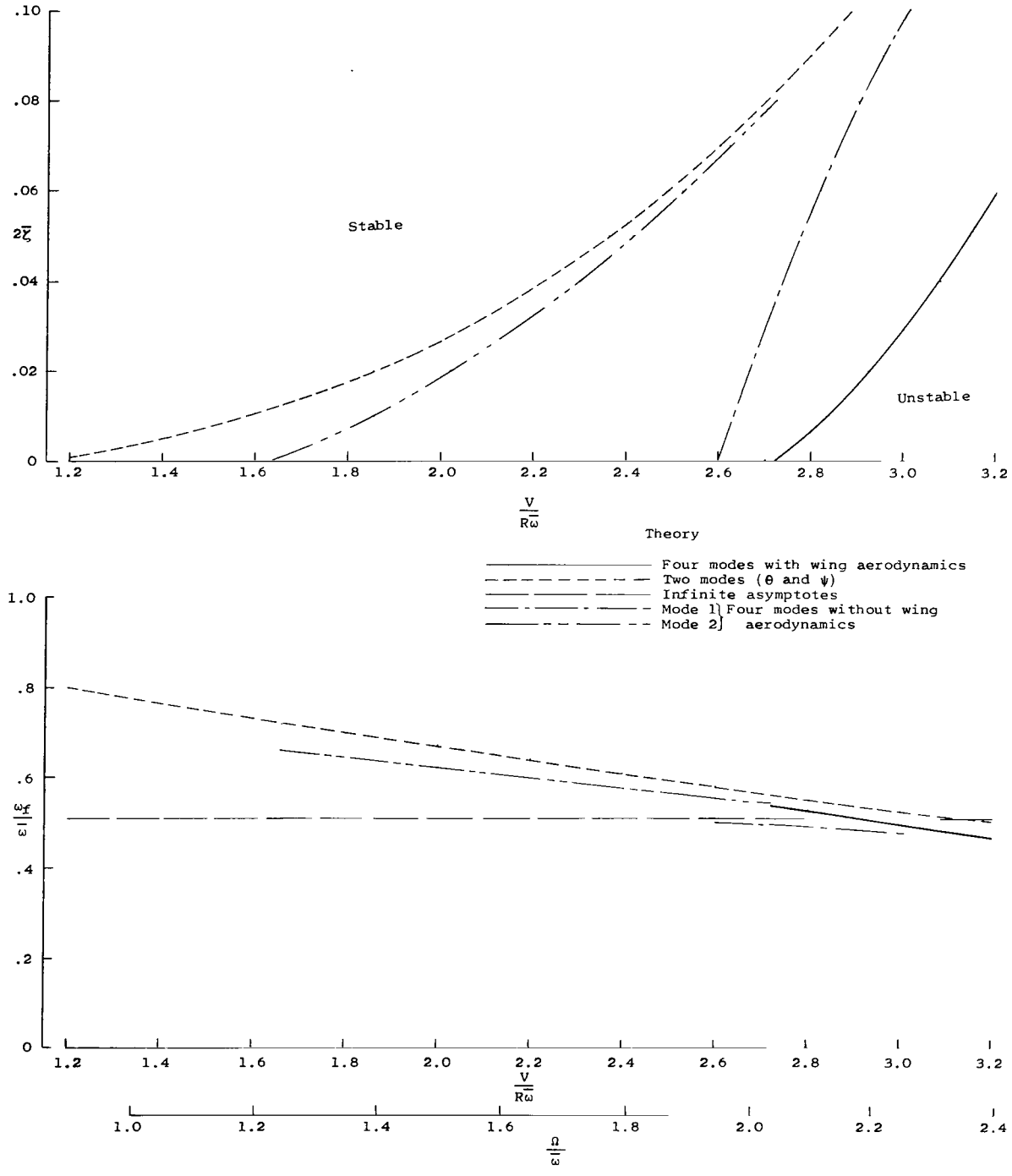

(c) $\beta_{0.75R} = 58^{\circ}$.

Figure 14.- Concluded.

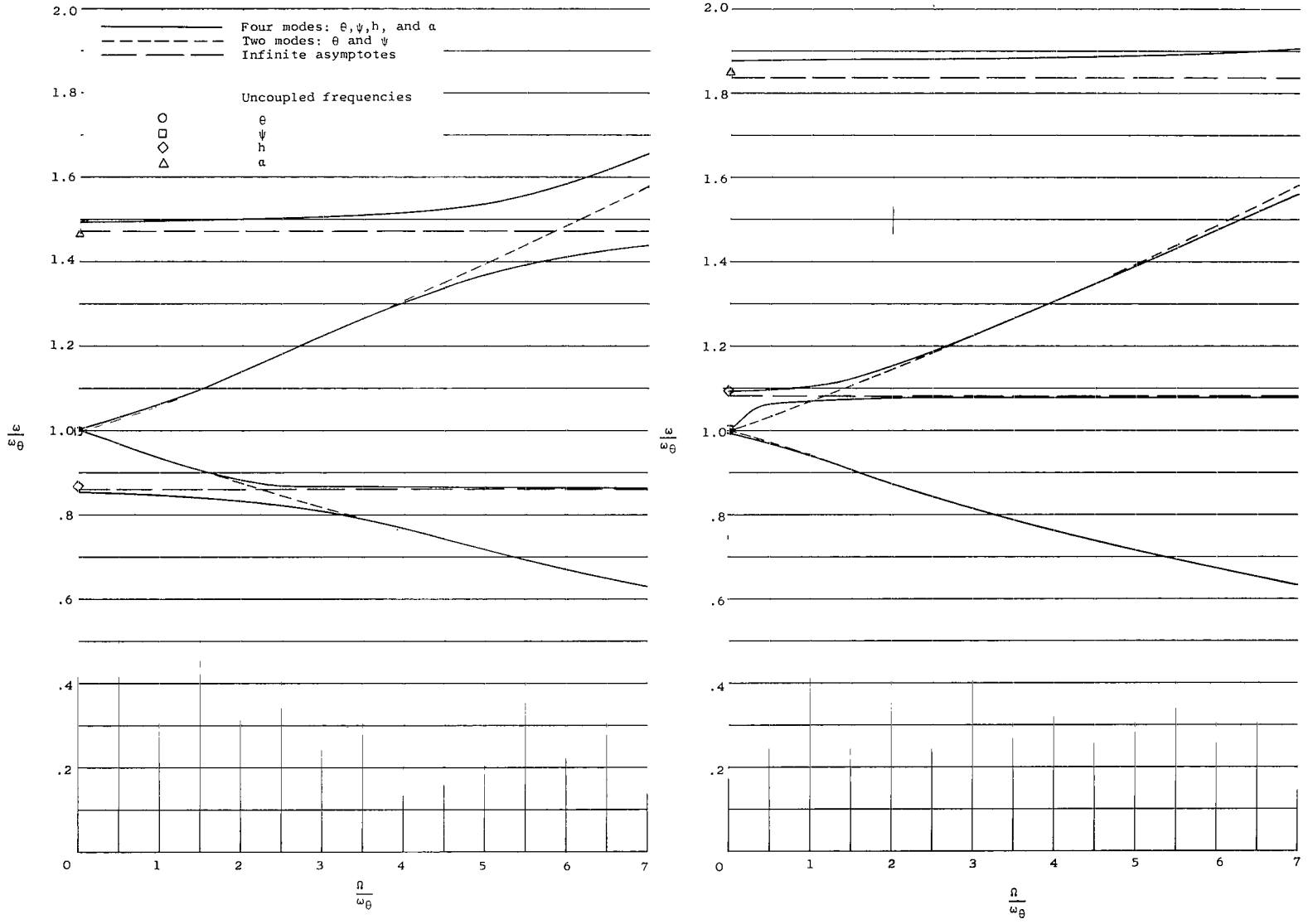

(a) Configuration A, f_θ = 11.65 cps.

(b) Configuration A, f_θ = 9.27 cps.

Figure 15.- The effect of propeller rotational speed on natural frequencies of vibration.

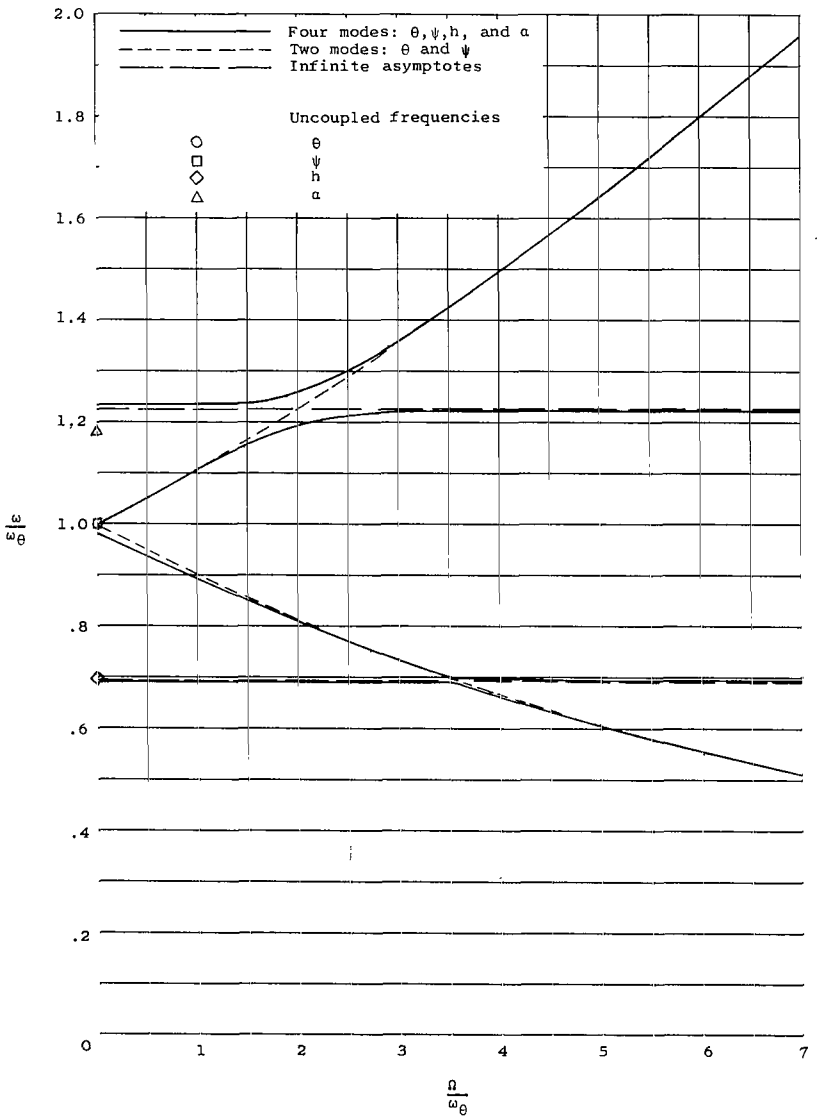

(c) Configuration B, f_θ = 14.5 cps.

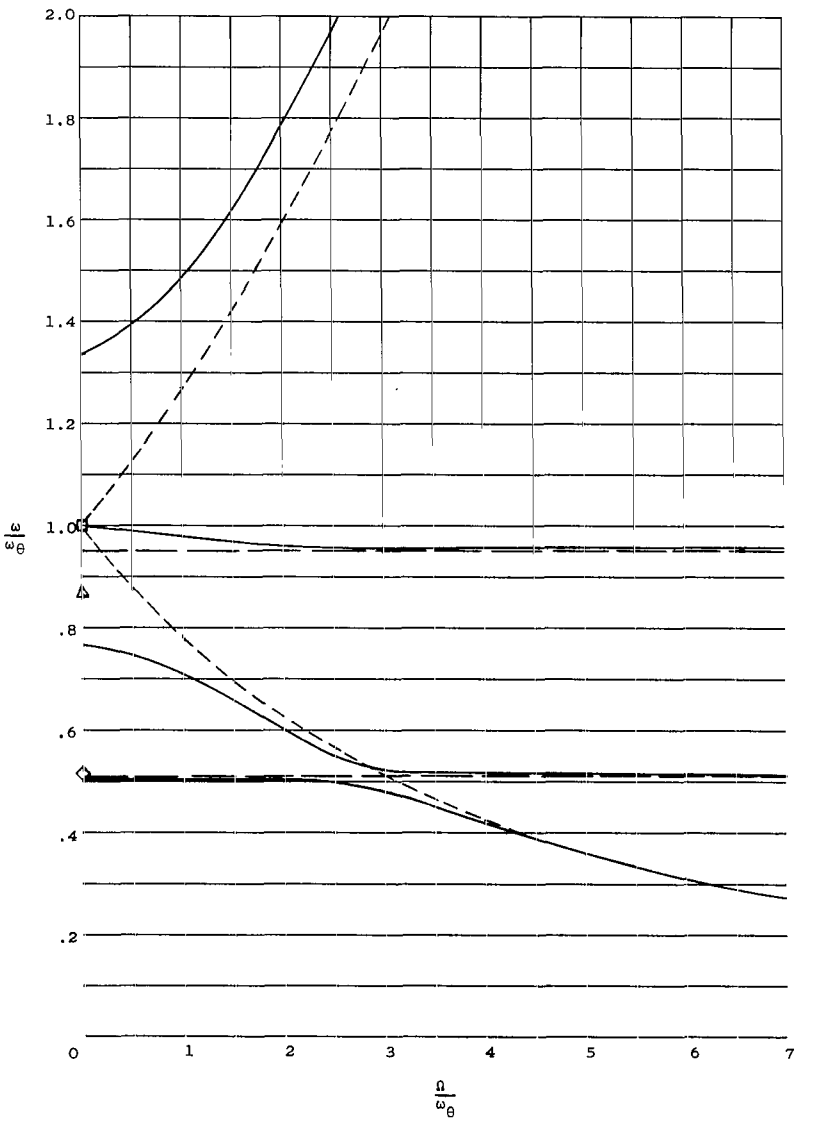

(d) Configuration C, f_θ = 19.7 cps.

Figure 15.- Continued.

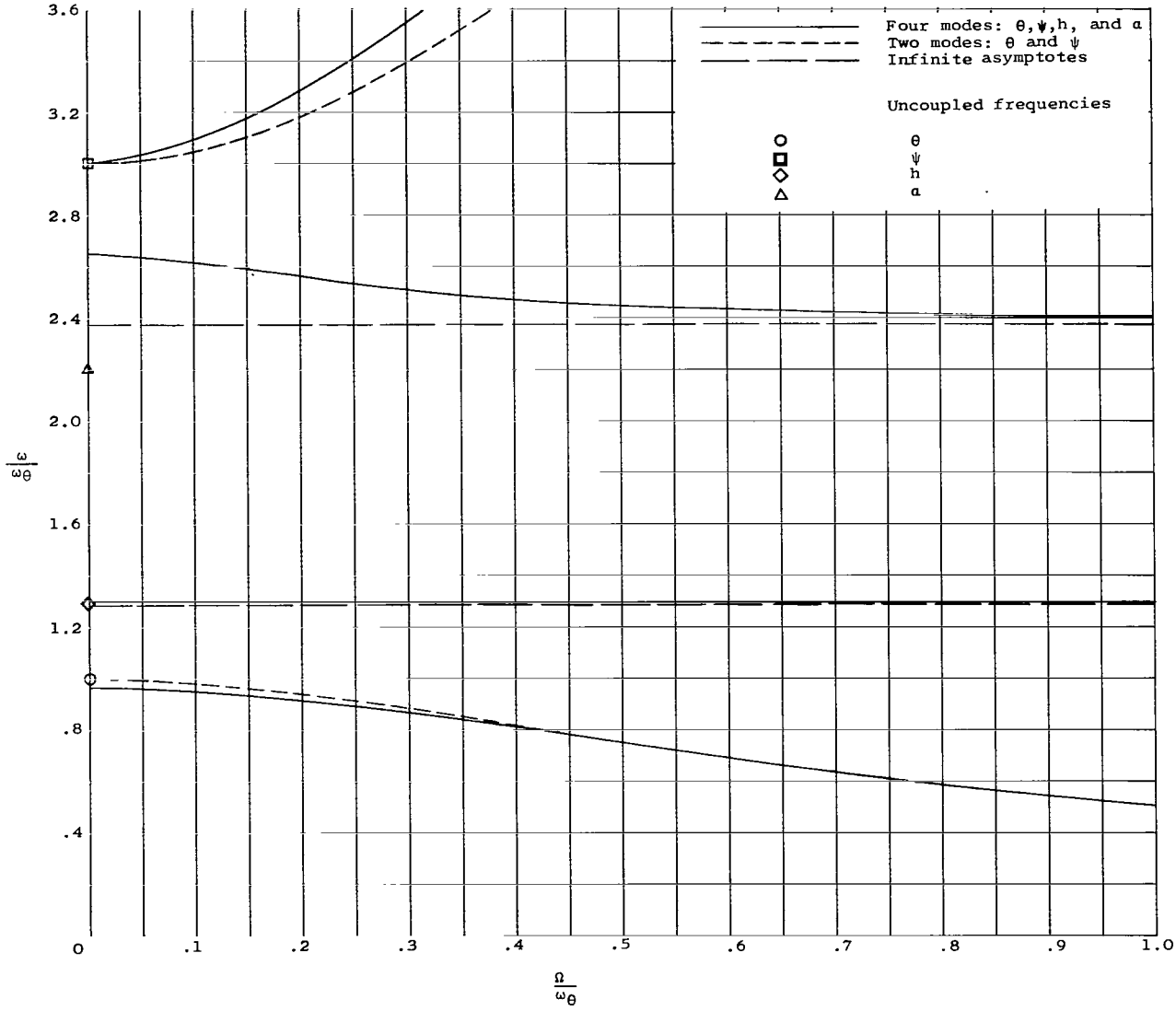

(e) Configuration D, f_θ = 7.80 cps.

Figure 15.- Concluded.

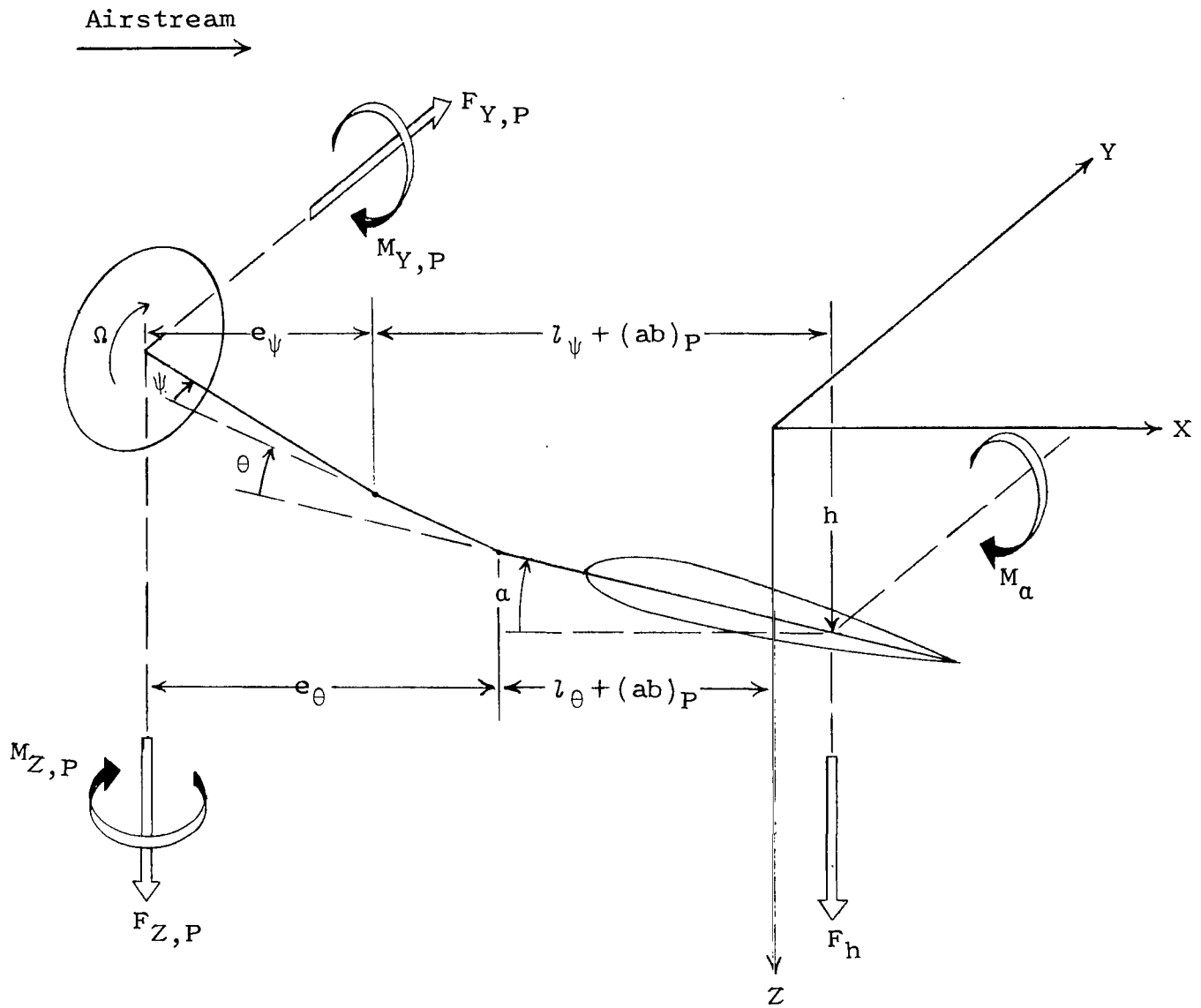

Figure 16.- Sketch showing directions of aerodynamic forces and moments.

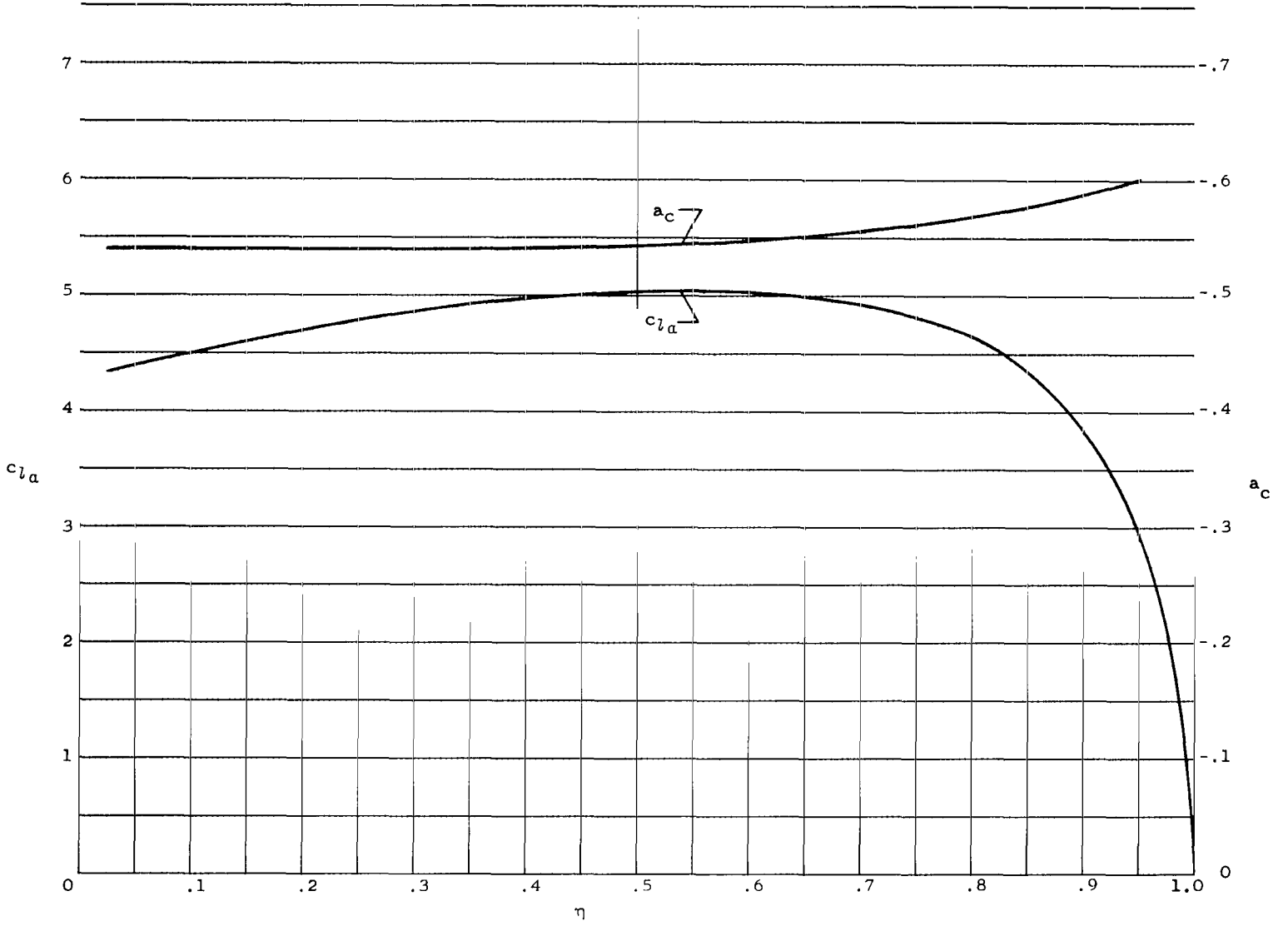

Figure 17.- Distribution of static aerodynamic parameters.

2/7/67

90

"The aeronautical and space activities of the United States shall be conducted so as to contribute . . . to the expansion of human knowledge of phenomena in the atmosphere and space. The Administration shall provide for the widest practicable and appropriate dissemination of information concerning its activities and the results thereof."

—NATIONAL AERONAUTICS AND SPACE ACT OF 1958

NASA SCIENTIFIC AND TECHNICAL PUBLICATIONS

TECHNICAL REPORTS: Scientific and technical information considered important, complete, and a lasting contribution to existing knowledge.

TECHNICAL NOTES: Information less broad in scope but nevertheless of importance as a contribution to existing knowledge.

TECHNICAL MEMORANDUMS: Information receiving limited distribution because of preliminary data, security classification, or other reasons.

CONTRACTOR REPORTS: Technical information generated in connection with a NASA contract or grant and released under NASA auspices.

TECHNICAL TRANSLATIONS: Information published in a foreign language considered to merit NASA distribution in English.

TECHNICAL REPRINTS: Information derived from NASA activities and initially published in the form of journal articles.

SPECIAL PUBLICATIONS: Information derived from or of value to NASA activities but not necessarily reporting the results of individual NASA-programmed scientific efforts. Publications include conference proceedings, monographs, data compilations, handbooks, sourcebooks, and special bibliographies.

Details on the availability of these publications may be obtained from:

SCIENTIFIC AND TECHNICAL INFORMATION DIVISION

NATIONAL AERONAUTICS AND SPACE ADMINISTRATION

Washington, D.C. 20546